Geoscientific
Model Development

Open Access

An integrated assessment modeling framework for uncertainty studies in global and regional climate change: the MIT IGSM-CAM (version 1.0)

E. Monier[1], J. R. Scott[1], A. P. Sokolov[1], C. E. Forest[2], and C. A. Schlosser[1]

[1]Joint Program on the Science and Policy of Global Change, Massachusetts Institute of Technology, Cambridge, Massachusetts, USA
[2]Department of Meteorology, Earth and Environmental Systems Institute, Pennsylvania State University, University Park, Pennsylvania, USA

Correspondence to: E. Monier (emonier@mit.edu)

Abstract. This paper describes a computationally efficient framework for uncertainty studies in global and regional climate change. In this framework, the Massachusetts Institute of Technology (MIT) Integrated Global System Model (IGSM), an integrated assessment model that couples an Earth system model of intermediate complexity to a human activity model, is linked to the National Center for Atmospheric Research (NCAR) Community Atmosphere Model (CAM). Since the MIT IGSM-CAM framework (version 1.0) incorporates a human activity model, it is possible to analyze uncertainties in emissions resulting from both uncertainties in the underlying socio-economic characteristics of the economic model and in the choice of climate-related policies. Another major feature is the flexibility to vary key climate parameters controlling the climate system response to changes in greenhouse gases and aerosols concentrations, e.g., climate sensitivity, ocean heat uptake rate, and strength of the aerosol forcing. The IGSM-CAM is not only able to realistically simulate the present-day mean climate and the observed trends at the global and continental scale, but it also simulates ENSO variability with realistic time scales, seasonality and patterns of SST anomalies, albeit with stronger magnitudes than observed. The IGSM-CAM shares the same general strengths and limitations as the Coupled Model Intercomparison Project Phase 3 (CMIP3) models in simulating present-day annual mean surface temperature and precipitation. Over land, the IGSM-CAM shows similar biases to the NCAR Community Climate System Model (CCSM)

version 3, which shares the same atmospheric model. This study also presents 21st century simulations based on two emissions scenarios (unconstrained scenario and stabilization scenario at 660 ppm CO_2-equivalent) similar to, respectively, the Representative Concentration Pathways RCP8.5 and RCP4.5 scenarios, and three sets of climate parameters. Results of the simulations with the chosen climate parameters provide a good approximation for the median, and the 5th and 95th percentiles of the probability distribution of 21st century changes in global mean surface air temperature from previous work with the IGSM. Because the IGSM-CAM framework only considers one particular climate model, it cannot be used to assess the structural modeling uncertainty arising from differences in the parameterization suites of climate models. However, comparison of the IGSM-CAM projections with simulations of 31 CMIP5 models under the RCP4.5 and RCP8.5 scenarios show that the range of warming at the continental scale shows very good agreement between the two ensemble simulations, except over Antarctica, where the IGSM-CAM overestimates the warming. This demonstrates that by sampling the climate system response, the IGSM-CAM, even though it relies on one single climate model, can essentially reproduce the range of future continental warming simulated by more than 30 different models. Precipitation changes projected in the IGSM-CAM simulations and the CMIP5 multi-model ensemble both display a large uncertainty at the continental scale. The two ensemble simulations show good agreement over Asia and Europe.

However, the ranges of precipitation changes do not overlap – but display similar size – over Africa and South America, two continents where models generally show little agreement in the sign of precipitation changes and where CCSM3 tends to be an outlier. Overall, the IGSM-CAM provides an efficient and consistent framework to explore the large uncertainty in future projections of global and regional climate change associated with uncertainty in the climate response and projected emissions.

1   Introduction

For many years, the Massachusetts Institute of Technology (MIT) Joint Program on the Science and Policy of Global Change has devoted a large effort to estimating probability density functions (PDFs) of uncertain inputs controlling human emissions and the climate response (Reilly et al., 2001; Forest et al., 2001, 2008). Based on these PDFs, probabilistic forecasts of the 21st century climate have been performed to inform policy-makers and the climate community at large (Sokolov et al., 2009; Webster et al., 2012). This effort has been organized around the MIT Integrated Global System Model (IGSM), an integrated assessment model that couples an Earth system model of intermediate complexity to a human activity model. The IGSM framework presents major advantages in the application of climate change studies. A fundamental feature of the IGSM is the ability to vary key parameters controlling the climate system response to changes in greenhouse gases and aerosols concentrations, e.g., the climate sensitivity, the strength of aerosol forcing and the rate of heat uptake by the ocean (Raper et al., 2002; Forest et al., 2008). Webster and Sokolov (2000) show that uncertainty in climate sensitivity associated with differences in parameterizations of physical processes used in different Atmosphere-Ocean Coupled General Circulation Models (AOGCMs) can be treated as an uncertainty in the cloud feedback adjustment factor. As such, the IGSM enables structural uncertainties to be treated as parametric ones and provides a flexible framework to analyze the effect of some of the structural uncertainties present in AOGCMs. The uncertainty in the carbon cycle is also taken into account in the IGSM by varying the rate of carbon uptake by the ocean and terrestrial ecosystem. Another major advantage of the IGSM is the coupling of the Earth system with a detailed economic model. This allows not only simulations of future climate change for various emissions scenarios to be carried out but also for the analysis of the uncertainties in emissions that result from uncertainties intrinsic to the economic model (Webster et al., 2012).

Since the IGSM includes a two-dimensional zonal-mean representation of the atmosphere, it has been used primarily for global mean climate change studies. While projections of future changes in the global mean climate remains a fundamental objective, probabilistic projections of future regional climate change would prove beneficial to policy-makers and

impact modeling research groups who investigate climate change and its societal impacts at the regional level, including agriculture productivity, water resources and energy demand (Reilly et al., 2013). The aim of the MIT Joint Program is to contribute to this effort by investigating regional climate change under uncertainty in the climate response and projected emissions. For studies requiring three-dimensional atmospheric capabilities, a new capability of the MIT Joint Program modeling framework is presented in which the IGSM is linked to the National Center for Atmospheric Research (NCAR) Community Atmosphere Model (CAM) version 3.

In this paper, we provide a description of the IGSM, including the Earth system model of intermediate complexity and the human activity model, and of the newly developed IGSM-CAM framework. Then, we compare IGSM-CAM and IGSM stand-alone historical simulations with observations and with models from the Coupled Model Intercomparison Project Phase 3 (CMIP3; Meehl et al., 2007b). We then present results from 21st century simulations based on two emissions scenarios (unconstrained emissions scenario and stabilization scenario at 660 ppm CO_2-equivalent by 2100) and three sets of climate parameters. The chosen climate parameters provide a good approximation for the median, and the 5th and 95th percentiles of the probability distribution of 21st century changes in surface air temperature. Thus, this study presents estimates of the median and 90 % probability interval of regional climate change for two different emissions scenarios. We then compare the range of projections with that of models from the Coupled Model Intercomparison Project Phase 5 (CMIP5, Taylor et al., 2012).

2   Modeling framework

2.1   The MIT IGSM framework

The MIT IGSM (Dutkiewicz et al., 2005; Sokolov et al., 2005) is an integrated assessment model that couples an Earth system model of intermediate complexity to a human activity model. The atmospheric dynamics and physics component (Sokolov and Stone, 1998) is a two-dimensional zonal-mean, statistical dynamical representation of the atmosphere at 4° resolution in latitude with eleven levels in the vertical. In version 2.2, the IGSM uses a two-dimensional mixed layer anomaly diffusive ocean model. In version 2.3, the ocean component includes a three-dimensional dynamical ocean component based on the MIT ocean general circulation model (Marshall et al., 1997) with a thermodynamic sea-ice model and an ocean carbon cycle (Dutkiewicz et al., 2005, 2009). The ocean model has a realistic bathymetry, and a 2° × 2.5° resolution in the horizontal with twenty-two layers in the vertical, ranging from 10 m at the surface to 500 m thick at depth. Heat and freshwater fluxes are anomaly coupled in order to simulate a realistic ocean state. In order

to more realistically capture surface wind forcing over the ocean, six-hourly National Centers for Environmental Prediction (NCEP) reanalysis 1 (Kalnay et al., 1996) surface 10 m wind speed from 1948–2007 is used to formulate wind stress. The data are detrended through analysis of changes in zonal mean over the ocean (by month) across the full 60 yr period; this has little impact except over the Southern Ocean, where the trend is quite significant (Thompson and Solomon, 2002). For any given model calendar year, a random calendar year of wind stress data is applied to the ocean. This approach ensures that both short-term weather variability and interannual variability are represented in the ocean's surface forcing. Different random sampling can be applied to simulate different natural variability, augmenting the traditional approach of specifying perturbations in initial conditions.

The IGSM also includes an urban air chemistry model (Mayer et al., 2000) and a detailed global scale zonal-mean chemistry model (Wang et al., 1998) that consider the chemical fate of 33 species including greenhouse gases and aerosols. The terrestrial water, energy and ecosystem processes are represented by the Global Land System (GLS) framework (Schlosser et al., 2007) that integrates three existing models: the NCAR Community Land Model (CLM) (Oleson et al., 2004), the Terrestrial Ecosystem Model (TEM) (Melillo et al., 1993) and the Natural Emissions Model (NEM) (Liu, 1996). The GLS framework represents biogeophysical characteristics and fluxes between land and atmosphere and estimates changes in terrestrial carbon storage and the net flux of carbon dioxide, as well as emissions of methane and nitrous oxide from terrestrial ecosystems.

Finally, the human system component of the IGSM is the MIT Emissions Predictions and Policy Analysis (EPPA) model version 4 (Paltsev et al., 2005), which provides projections of world economic development and emissions over 16 global regions along with an analysis of proposed emissions control measures. EPPA is a recursive-dynamic multi-regional general equilibrium model of the world economy, which is built on the Global Trade Analysis Project (GTAP) data set of the world economic activity (maintained at Purdue University) augmented by data on the emissions of greenhouse gases, aerosols and other relevant species, and details of selected economic sectors. The model projects economic variables (gross domestic product, energy use, sectoral output, consumption, etc.) and emissions of greenhouse gases (CO_2, CH_4, N_2O, HFCs, PFCs and SF_6) and other air pollutants (CO, VOC, NO_x, SO_2, NH_3, black carbon and organic carbon) from combustion of carbon-based fuels, industrial processes, waste handling and agricultural activities.

Since the IGSM includes a human activity model, it can be used to examine the impact of different climate policies on emissions of greenhouse gases and aerosols and on future climate change within a single consistent framework. Another major feature of the IGSM is the flexibility to vary key climate parameters controlling the climate response. The climate sensitivity can be changed by varying the cloud feedback (Sokolov, 2006) while the strength of the aerosol forcing is modified by adjusting the total sulfate aerosol radiative forcing efficiency. In the IGSM2.3, the rate of ocean heat uptake can be changed by modifying the value of the diapycnal diffusion coefficient (Dalan et al., 2005), resulting in multiple versions of the IGSM2.3 with different ocean heat uptake rates. The IGSM is also computationally efficient and thus particularly adapted to conduct sensitivity experiments or to allow for several millennia long simulations. The IGSM has been used in EMIC intercomparison exercises (Gregory et al., 2005; Petoukhov et al., 2005; Brovkin et al., 2006; Stouffer et al., 2006; Plattner et al., 2008; Eby et al., 2013; Zickfeld et al., 2013) as well as to quantify the PDFs of climate parameters using optimal fingerprint detection statistics (Forest et al., 2001, 2008). This is accomplished by comparing observed changes in surface, upper-air, and deep-ocean temperature changes against IGSM simulations of 20th century climate where model parameters are systematically varied. The IGSM has also been used to make probabilistic projections of 21st century climate change under varying emissions scenarios and climate parameters (Sokolov et al., 2009; Webster et al., 2012) and to investigate the ocean circulation response to climate change (Scott et al., 2008).

2.2 The IGSM-CAM framework

Because the atmospheric component of the IGSM is two-dimensional (zonally averaged), regional climate cannot be directly resolved. For investigations requiring three-dimensional atmospheric capabilities, the IGSM2.3 is linked to CAM version 3 (Collins et al., 2004), at a $2° \times 2.5°$ horizontal resolution with 26 vertical levels. Figure 1 shows the schematic of the IGSM-CAM (version 1.0) framework. The IGSM version 2.3 is preferred over version 2.2 because of the ability of the three-dimensional dynamical ocean component to more accurately simulate ocean dynamics and regional variability. CAM3 is chosen over different atmospheric models because it is coupled to CLM, and thus provides a biogeophysical representation of the land consistent with the IGSM. For further consistency within the IGSM-CAM framework, new modules were developed and implemented in CAM in order to change its climate parameters to match those of the IGSM. In particular, the climate sensitivity is changed using a cloud radiative adjustment method (Sokolov and Monier, 2012). CAM is driven by greenhouse gases concentrations and aerosols loading simulated by the IGSM model. Since the IGSM only computes a 2-D zonal-mean distribution of aerosols, we use a pattern scaling method in order to provide CAM with a 3-D distribution of aerosols. Since CAM provides a scaling option for carbon aerosols, the default 3-D black carbon aerosols loading is scaled to match the global carbon mass in the IGSM. A similar scaling for sulfate aerosols was implemented in CAM and the default 3-D sulfate aerosols loading is scaled so that the sulfate aerosol radiative forcing matches that of the IGSM. The
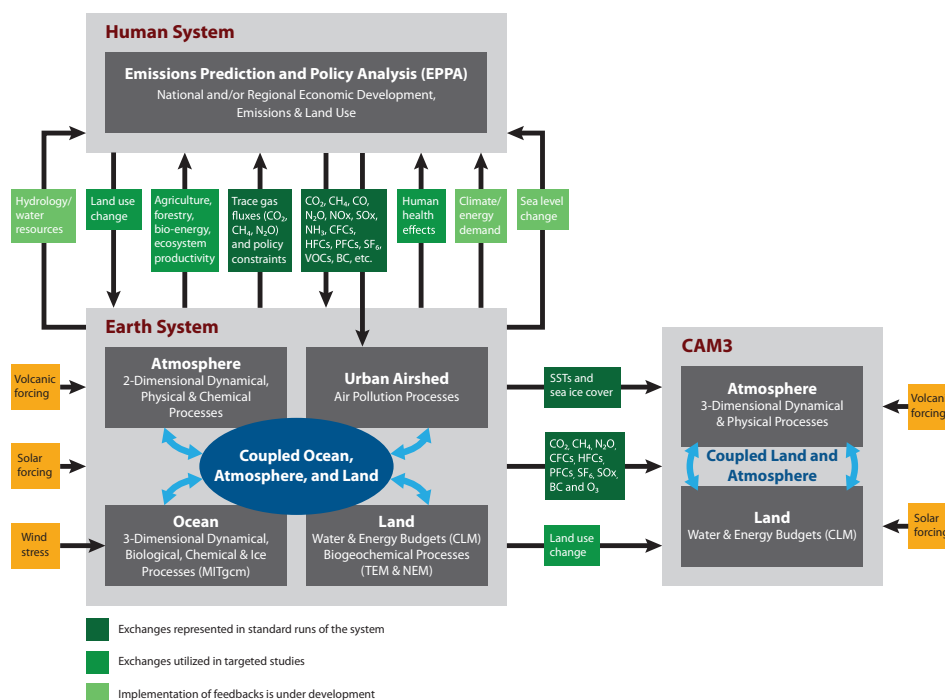
Fig. 1. Schematic of the IGSM-CAM framework highlighting the coupled linkages between the physical and socio-economic components of the IGSM2.3 and the linkage between the IGSM and CAM.

ozone concentrations driving CAM are a combination of the IGSM zonal-mean distribution of ozone in the troposphere and of stratospheric ozone concentrations derived from the Model for Ozone and Related Chemical Tracers (MOZART, Horowitz et al., 2003). Finally, CAM is driven by monthly IGSM sea surface temperature (SST) anomalies from a control simulation corresponding to pre-industrial forcing added to monthly mean climatology (over the 1870–1880 period) taken from the merged Hadley-OI SST, a surface boundary data set designed for uncoupled simulations with CAM (Hurrell et al., 2008). Not surprisingly, the IGSM SSTs exhibit regional biases, due to the lack of representation of storm tracks and other inherent limitations of coupling the ocean with a 2-D atmosphere. These biases are present in the seasonal cycle of the ocean state but SST anomalies from, for example, the pre-industrial mean agree well with observed anomalies. For this reason, CAM is driven by the IGSM SST anomalies and not the full SSTs. More details on the IGSM SST bias are given in the Supplement.

The IGSM-CAM provides an efficient method to estimate uncertainty in global and regional climate change. First, the IGSM-CAM can make use of the IGSM probabilistic ensemble projections and can then subsample them at key quantile values (e.g., 5th and 95th percentile, median) to obtain a first-order assessment of regional uncertainties without necessarily having to run the entire set of members (in the order of several hundred simulations) from the IGSM ensemble. Second, since the atmospheric chemistry and the land and

ocean biogeochemical cycles are computed within the computationally efficient IGSM (and not in the 3-dimensional atmospheric model), the IGSM-CAM is more computationally efficient than a fully coupled GCM, like the NCAR Community Climate System Model (CCSM). On the other hand, the current version of the IGSM-CAM does not consider potential changes in the spatial distribution of aerosols and ozone. In future versions, the spatial distribution of ozone and aerosols will be modified spatially as a function of the change in the emissions distribution, computed in the human system component of the IGSM-CAM. Nonetheless, the IGSM-CAM version 1.0 provides a framework well adapted for uncertainty studies in global and regional climate change since the key parameters that control the climate system response (climate sensitivity, strength of aerosol forcing and ocean heat uptake rate) can be varied consistently within the modeling framework.

3   Description of the simulations

In this study, results from simulations with two emissions scenarios and three sets of climate parameters are presented. For each set of climate parameters and emissions scenarios, a five-member ensemble is run with different random wind sampling and initial conditions, referred to as simply initial conditions in the remainder of the article, in order to account for the uncertainty in natural variability, resulting in a total of 30 simulations.
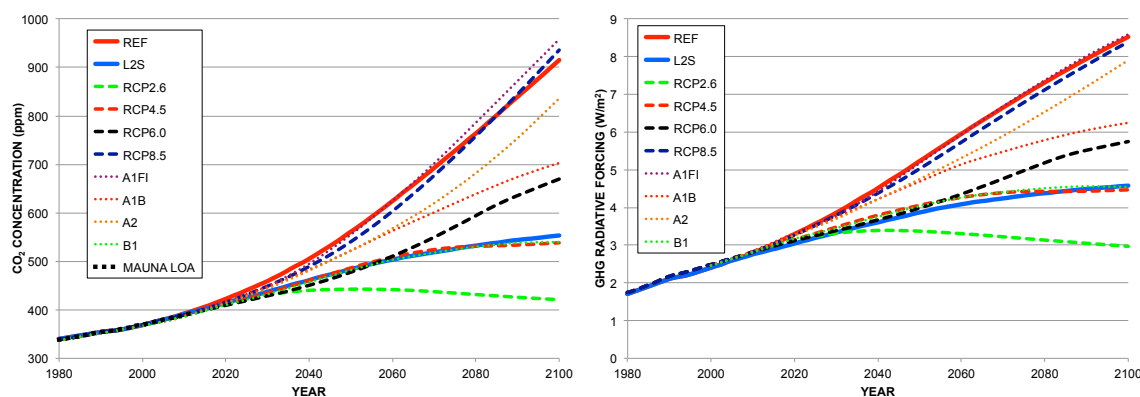
Fig. 2. Global mean (left) CO_2 concentrations (ppm) and (right) greenhouse gases radiative forcing (W m^{-2}) for the REF and L2S scenarios, the A1FI, A1B, A2 and B1 SRES scenarios and the RCP2.6, RCP4.5, RCP6.0 and RCP8.5 scenarios. Observed CO_2 concentrations at Mauna Loa are also shown.

3.1 Emissions scenarios

The two emissions scenarios presented in this study are a median unconstrained reference scenario where no policy is implemented after 2012, referred to as REF, and a stabilization scenario that corresponds to the level 2 stabilization (L2S) described in Clarke et al. (2007), where greenhouse gases are stabilized at 660 ppm CO_2-equivalent (550 ppm CO_2-only) by 2100 (see Fig. 2). These emissions are similar to, respectively, the Representative Concentration Pathways RCP8.5 and RCP4.5 scenarios (Moss et al., 2010). The median unconstrained reference scenario corresponds to the median of the distribution obtained by performing Monte Carlo simulations of the EPPA model, using Latin Hypercube sampling of 100 parameters, resulting in a 400-member ensemble simulation of the economic model (Webster et al., 2008). As opposed to the Special Report on Emissions Scenarios (SRES, Nakicenovic et al., 2000) and RCP scenarios, this approach allows a more structured development of scenarios that are suitable for uncertainty analysis of an economic system that results in different emissions profiles. Usually the EPPA scenario construction starts from a reference scenario under the assumption that no climate policies are imposed. Then additional stabilization scenarios framed as departures from its reference scenario are achieved with specific policy instruments. The 660 ppm CO_2-equivalent stabilization scenario is achieved with a global cap and trade system with emissions trading among all regions beginning in 2015. The path of the emissions over the whole period (2015–2100) was constrained to simulate cost-effective allocation of abatement over time. More details on the emissions scenarios used in this study can be found in Clarke et al. (2007).
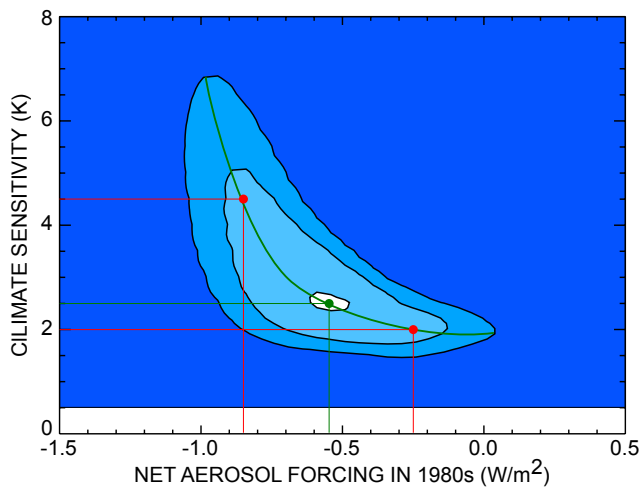
3.2 Climate parameters

Different versions of the IGSM2.3 exist with different values of the diapycnal diffusion coefficient. The corresponding effective vertical diffusion is computed using the methodology

described in Sokolov et al. (2003). In this study, we pick the version of the IGSM2.3 with a rate of ocean heat uptake that corresponds to an effective vertical diffusion of 0.5 cm^2 s^{-1}, which lies between the mode and the median of the probability distribution obtained with the IGSM using optimal fingerprint detection statistics (Forest et al., 2008). Following a methodology similar to Forest et al. (2008), we compute the bivariate marginal posterior probability density function with uniform prior for the climate sensitivity-net aerosol forcing (CS-F_{aer}) parameter space (Fig. 3). We choose three values of climate sensitivity (CS) that correspond to the 5th percentile (CS = 2.0 °C), median (CS = 2.5 °C), and 95th percentile (CS = 4.5 °C) of the marginal posterior probability density function with uniform prior (integrated over the net aerosol forcing). The lower and upper bounds of climate sensitivity agree well with the conclusions of the Fourth Intergovernmental Panel on Climate Change (IPCC) Assessment Report (AR4) that finds that the climate sensitivity is likely to lie in the range of 2.0 to 4.5 °C (Hegerl et al., 2007). The value of the net aerosol forcing is then chosen from the CS-F_{aer} probability density function, with the objective to provide the best agreement with the observed 20th century climate change. The values for the net aerosol forcing are −0.25 W m^{-2}, −0.55 W m^{-2} and −0.85 W m^{-2}, respectively, for CS = 2.0 °C, CS = 2.5 °C, CS = 4.5 °C. Global climate changes obtained in these simulations provide a good approximation for the median and the 5th and 95th percentiles of the probability distribution of 21st century changes in surface air temperature from previous work with the IGSM.

4 Data sets

While CAM3 has been the subject of extensive validation (Hurrell et al., 2006; W. D. Collins et al., 2006), the IGSM-CAM framework needs to be evaluated for its ability to simulate the present climate state as well as past observed

Fig. 3. The marginal posterior probability density function with uniform prior for the climate sensitivity-net aerosol forcing (CS-F_{aer}) parameter space. The shading denotes rejection regions for a given significance level – 90 %, 10 % and 1 %, light to dark, respectively. The positions of the red and green dots represent the parameters used in the simulations presented in this study. The green line represents combinations of climate sensitivity and net aerosol forcing leading to the same 20th century global mean temperature changes as the median set of parameters (green dot).

changes. First the IGSM-CAM is compared to the IGSM2.3 stand-alone (for the remainder of the article, unless indicated otherwise, when the IGSM is mentioned, we refer to version 2.3) and evaluated against a large number of observational data sets and the CMIP3 models. The various observational data sets used in this study are: HadISST (Rayner et al., 2003), CRU surface temperature (Jones et al., 1999), CRUTEM4 (Jones et al., 2012), HadCRUT4 (Morice et al., 2012), 20th Century Reanalysis (20CR) V2 (Compo et al., 2011), Global Precipitation Climatology Project (GPCP) version 2.2 (Adler et al., 2003), Climate Prediction Center (CPC) Merged Analysis of Precipitation (CMAP) data set (Xie and Arkin, 1997), ERA-Interim (Dee et al., 2011), NCEP reanalysis 1 (Kalnay et al., 1996) and the newly developed global reconstructed precipitation (REC) data (Smith et al., 2012). When comparing the IGSM and IGSM-CAM simulations with observations, the simulations with the median climate sensitivity are chosen. Simulations with a different choice of climate sensitivity yield very similar results since the other values of climate parameters are chosen to best reproduce the observed 20th century climate change. Then, future projections of surface air temperature and precipitation are compared to 31 CMIP5 models (the list of the 31 CMIP5 models available at the time of the study is given in the Supplement).

5 Results

### 5.1 Evaluation of the present-day climate

Figures 4 and 5 show present-day (1981–2010 period) latitude-height cross sections of temperature and relative humidity for the IGSM, IGSM-CAM and two reanalysis products (ERA-Interim and NCEP reanalysis 1). The IGSM simulation displays a strong cold bias in the stratosphere and near-surface polar regions, and a small cold bias elsewhere. This cold bias is also present in the GISS atmospheric model (Hansen et al., 1983), from which the IGSM atmosphere is derived. The IGSM also shows a strong moist bias, in particular in the stratosphere and over the tropics. The moist bias in the tropics is likely due to the well-mixed 2-D zonal-mean atmosphere that overestimates relative humidity over land. In comparison, the IGSM-CAM simulation shows significant improvement over the IGSM simulation. The general cold bias in the IGSM is largely reduced, except in the stratospheric polar regions. Furthermore, the relative humidity simulated in the IGSM-CAM shows reasonable agreement with the reanalyses, especially in the tropics and in the stratosphere. The largest disagreement between the IGSM-CAM and the observations takes place where the two reanalyses tend to show the most discrepancies, e.g., relative humidity in the polar regions.

Figure 6 shows the present-day (1981–2010 period) latitudinal distribution of zonal-mean annual mean surface air temperature and precipitation for the IGSM and IGSM-CAM simulations and for observational data (20CR V2 and HadCRUT4 for temperature and 20CR V2 and GPCP v2.2 for precipitation). Generally, the IGSM-CAM simulation shows better agreement with the observations than the IGSM simulation. For temperature, the IGSM-CAM displays a strong agreement with the 20CR from 50° S to 60° N. The agreement is not as good over the polar regions, where there is also a strong disagreement between the 20CR and HadCRUT4 data sets. For precipitation, the IGSM-CAM simulates a realistic distribution of precipitation, with local maxima in the tropics, away from the equator, and at mid-latitudes. However, mid-latitude precipitation tends to span narrower bands than in the observations, with precipitation being underestimated in the 30–45° latitudinal bands. Nonetheless, the IGSM-CAM simulation of precipitation is improved over the IGSM, which displays weak mid-latitude precipitation.

Figure 7 shows the observed annual-mean merged SST and surface air temperature over land (CRU and HadISST) along with the IPCC AR4 multi-model mean error, the typical IPCC AR4 model error, and the CCSM3 and IGSM-CAM model errors. While comparing a single model with the IPCC AR4 multi-model mean is useful, in most cases, the multi-model mean is better than all of the individual models (Gleckler et al., 2008; Annan and Hargreaves, 2011). For this reason it is important to consider the typical error as an additional means of comparison and validation of the modeling
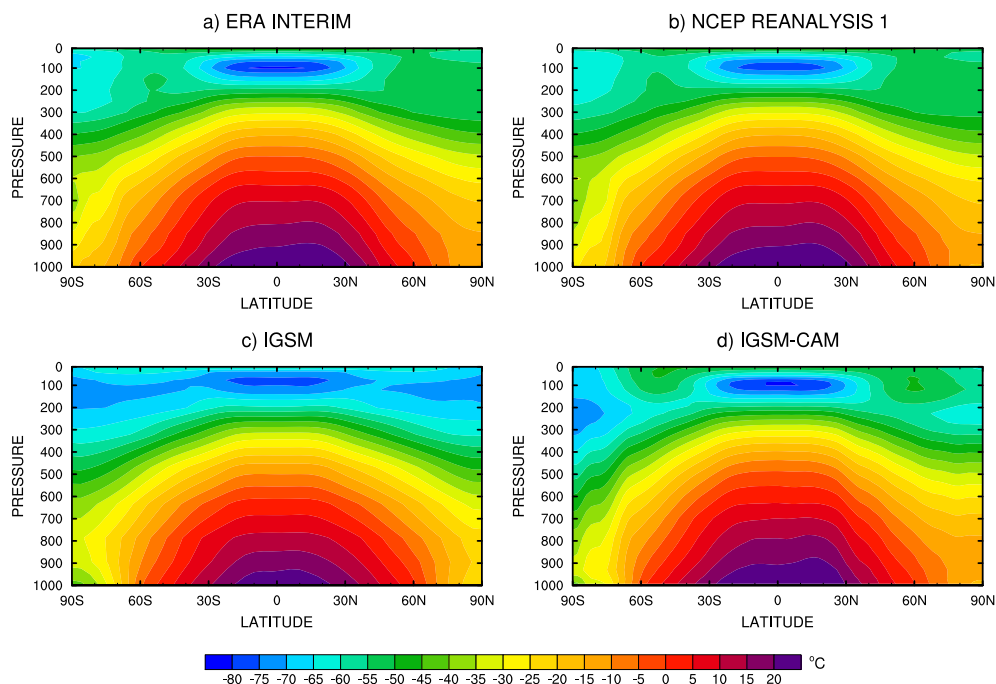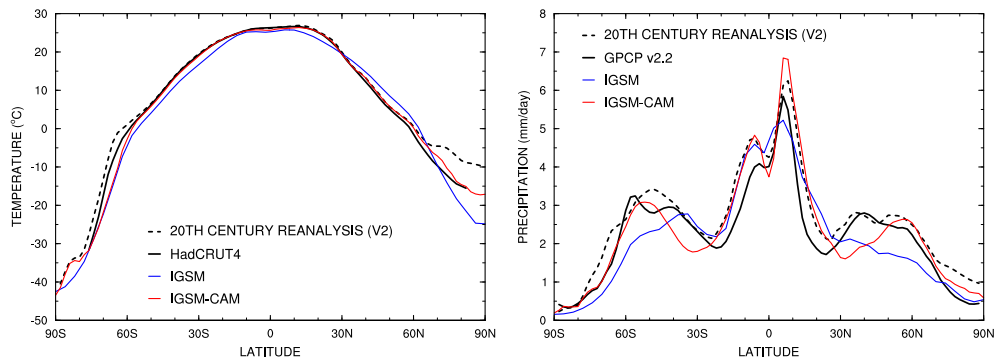
Fig. 4. Zonal mean vertical cross sections of present-day (1981–2010 period) temperature (°C) for the IGSM and IGSM-CAM simulations, under median climate sensitivity, and for the ERA-Interim and NCEP Reanalysis 1.
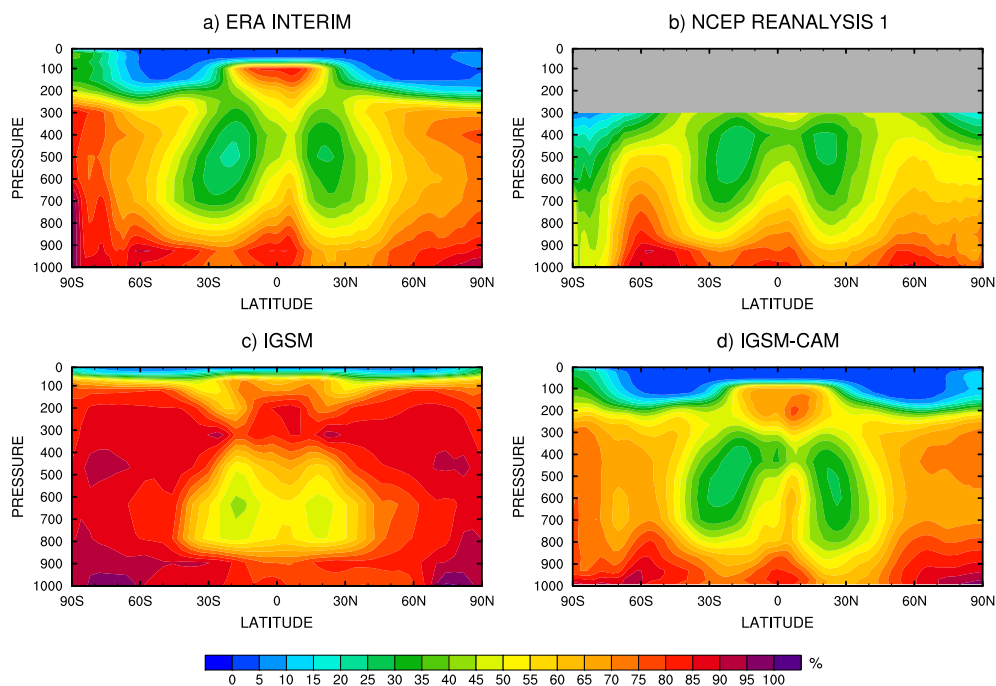
Fig. 5. Same as Fig. 4 but for relative humidity (%).

framework. The IGSM-CAM is also compared to CCSM3 because they share the same atmospheric model. As a result, a direct comparison with CCSM3 is useful to determine if these models share the same biases. Figure 7 reveals that the IGSM-CAM surface temperature error compares well

with the multi-model mean error over most of the globe and is generally within the typical error. The IGSM-CAM surface temperature agrees particularly well with observations over the ocean, with errors less than 1 °C. The close match over the ocean is a reflection of the IGSM-CAM anomaly

Fig. 6. Latitudinal distribution of present-day (1981–2010 period) zonal-mean (left) surface air temperature (°C) and (right) precipitation (mm day^{-1}) for the IGSM and IGSM-CAM simulations, under median climate sensitivity, and for two sets of observational data: HadCRUT4 and 20CR V2 for temperature, and GPCP v2.2 and 20CR V2 for precipitation.

coupling approach discussed in Sect. 2.2, whereas CCSM3 is fully coupled and would be expected to have larger SST errors. Over land areas, the IGSM-CAM generally exhibits regional biases similar to CCSM3. For example, the Great Lakes region and northern Eurasia suffer from a warm bias, while a cold bias is present over the Sahara and Sahel, caused by low column water vapor (Dickinson et al., 2006). The IGSM-CAM tends to be globally warmer than CCSM3 and thus shows exacerbated warm regional biases and reduced cold regional biases compared to CCSM3. Nonetheless, the largest errors in surface temperature are generally located in areas where the IPCC AR4 typical error is large. Such typical biases include warm biases over Antarctica, the Canadian Arctic region and eastern Siberia along with cold biases over the coast of Antarctica and the Himalayas. These errors are generally associated with polar regions, where biases in the simulated sea-ice have large impacts on surface temperature, and near topography that is not realistically represented at the resolution of the model.

Figure 8 shows a similar analysis for precipitation. The IGSM-CAM is generally able to simulate the major regional characteristics shown in the CMAP annual mean precipitation, including the lower precipitation rates at higher latitudes and the rainbands associated with the Intertropical Convergence Zone (ITCZ) and mid-latitude oceanic storm tracks. Nonetheless, the IGSM-CAM model error shows regional biases with patterns generally similar to the mean IPCC AR4 model error over the ocean, but with larger magnitudes. Like in the IPCC AR4 mean model, the IGSM-CAM precipitation presents a wet bias in the western basin of the Indian Ocean and a dry bias in the eastern basin. The IGSM-CAM and the IPCC AR4 mean model also show similar biases in precipitation patterns over the Pacific and Atlantic Ocean. Over the extratropical region (in particular in the 30–45° latitudinal bands), the dry bias in the IGSM-CAM described earlier is also present in the IPCC AR4 mean model and CCSM3. The typical IPCC AR4 model error reveals that many of the IPCC AR4 models display substantial

precipitation biases, especially in the tropics, which often approach the magnitude of the observed precipitation (Randall et al., 2007). Over land, the IGSM-CAM model error displays regional biases very similar to CCSM3. For example, the Amazon Basin tends to be too dry (Dickinson et al., 2006) and so does the Gulf Coast of the United States and Southeast Asia. Meanwhile, a wet bias can be seen over Central Africa in both CCSM3 and the IGSM-CAM.

The IGSM-CAM tends to simulate more realistically the present-day climatology of temperature, relative humidity and precipitation than the IGSM. This is not entirely surprising considering that the IGSM includes an Earth system model of intermediate complexity with a 2-D zonal-mean atmosphere. While the IGSM 2-D atmosphere includes parameterizations of heat, moisture, and momentum transports by large-scale eddies, it cannot accurately simulate the ocean/land contrasts and atmospheric circulations. As a result, the addition of a 3-D atmospheric component shows substantial improvements. As a result, the IGSM-CAM shares the same general strengths and limitations as the CMIP3 models in simulating present-day annual mean surface temperature and precipitation. Over land, the IGSM-CAM model error in surface temperature and precipitation are very similar to CCSM3, indicating that the two models share biases and that model errors within CAM are likely to propagate in IGSM-CAM climate projections. In addition, the substantial biases in the simulated present-day precipitation can explain the lack of consensus in the sign of future regional precipitation changes predicted by IPCC AR4 models in many regions of the world. However, a model does not necessarily require a realistic simulation of the present mean state to accurately simulate past trends and presumably future trends, as demonstrated in Eby et al. (2013).

5.2 Evaluation of the variability

Figures 9 and 10 show Hovmöller diagrams of surface air temperature and precipitation anomalies over the 1900–2010
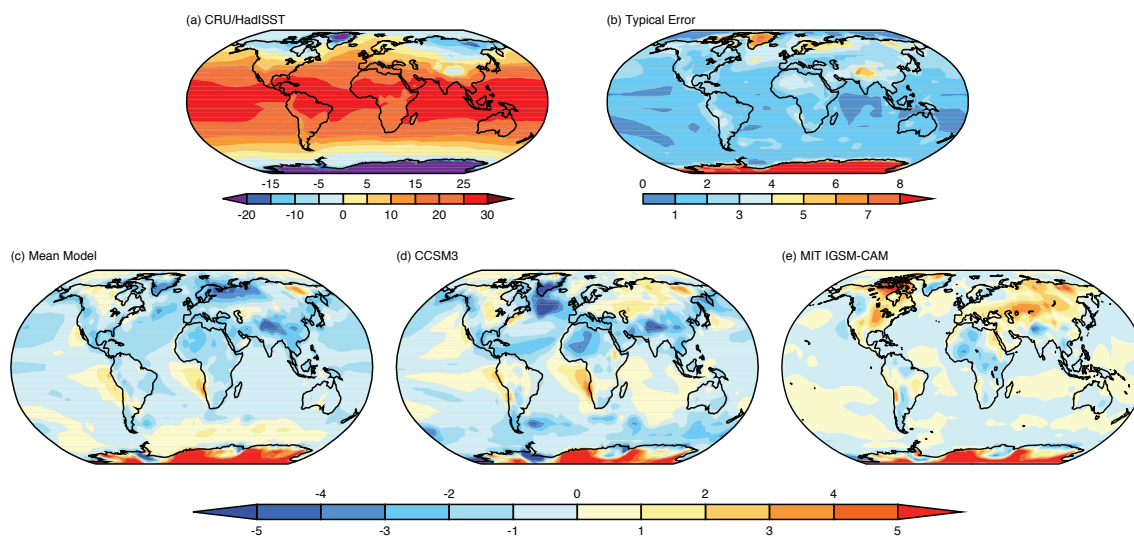
Fig. 7. (a) Observed annual-mean HadISST1 climatology for 1980–1999 and CRU surface air temperature climatology over land for 1961–1990; **(b)** root-mean-square model error (°C), based on all available IPCC model simulations (i.e., square-root of the sum of the squares of individual model errors, divided by the number of models); **(c)** IPCC AR4 multi-model mean error (°C), simulated minus observed; (d) CCSM3 model error (°C), simulated minus observed; and **(e)** IGSM-CAM model error (°C), under median climate sensitivity, simulated minus observed. The model results are for the same period as the observations. In the presence of sea ice, the SST is assumed to be at the approximate freezing point of sea water ($-1.8\,°C$). Adapted from Randall et al. (2007), Fig. S8.1b.
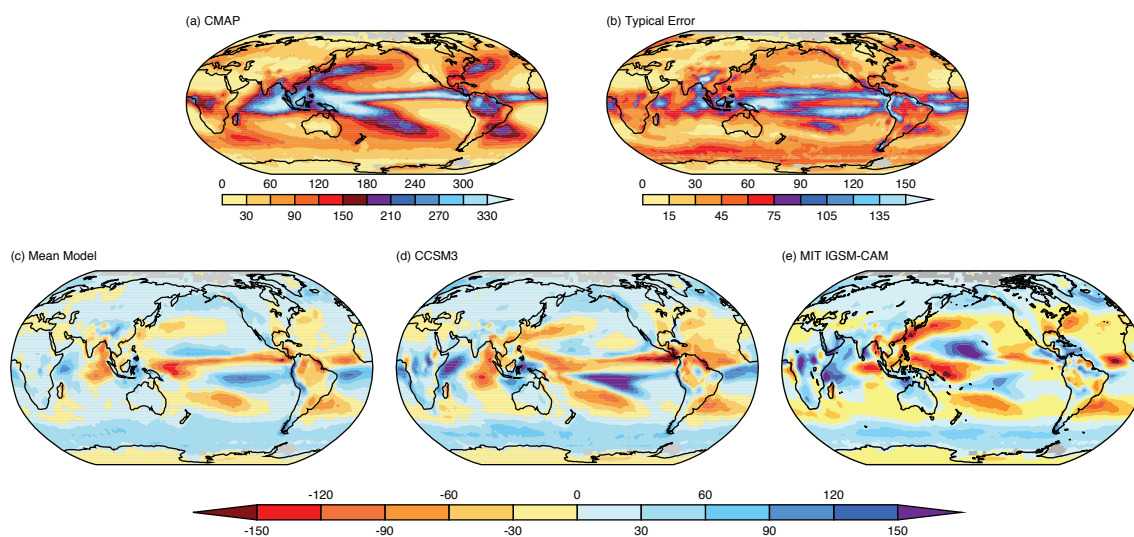
Fig. 8. (a) Observed annual-mean CMAP precipitation climatology for 1980–1999 (cm); **(b)** root-mean-square model error (cm), based on all available IPCC model simulations (i.e., square-root of the sum of the squares of individual model errors, divided by the number of models); **(c)** IPCC AR4 multi-model mean error (cm), simulated minus observed; and **(d)** CCSM3 model error (cm), simulated minus observed; and **(e)** IGSM-CAM model error (cm), under median climate sensitivity, simulated minus observed. The model results are for the same period as the observations. Observations were not available in the gray regions. Adapted from Randall et al. (2007), Fig. S8.9b.

period for the IGSM and IGSM-CAM simulations and for a set of two observational data sets, one based on station data or satellite measurements (HadCRUT4 for temperature and GPCP v2.2 for precipitation), the other being a reanalysis product (20CR V2 for both temperature and precipitation). Both IGSM and IGSM-CAM simulations show a

realistic increase in the zonal-mean surface air temperature over the period considered, which the largest increase in the polar regions. They also display a distinct year-to-year variability in the tropics, consistent with the two observational data sets. However, the IGSM-CAM simulates a larger and more realistic year-to-year variability in the polar regions
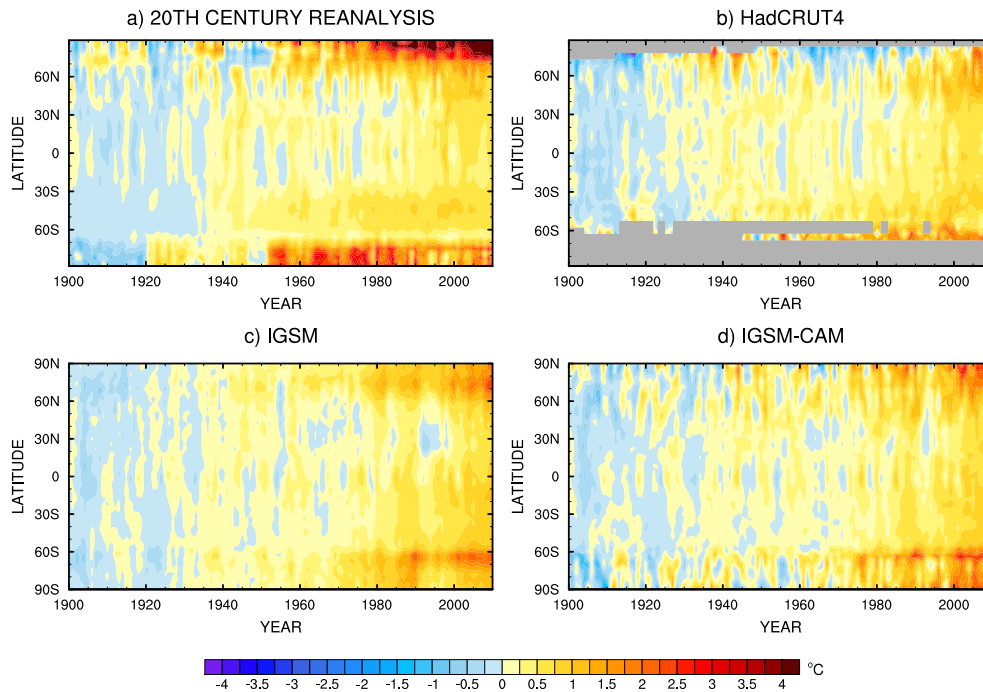
Fig. 9. Hovmöller diagrams of zonal-mean surface air temperature anomalies from the 1901–1950 mean (°C) for the IGSM and IGSM-CAM simulations, under median climate sensitivity, and for the HadCRUT4 and 20CR V2.

than the IGSM. Generally, the IGSM and IGSM-CAM simulations differ the most from the observations at high latitudes, where the two observational data sets show the least amount of agreement. In terms of precipitation, the IGSM-CAM presents a significant improvement over the IGSM, in particular outside of the tropics where the IGSM simulation shows very little variability. In addition, the spatial and temporal coherency of the IGSM-CAM precipitation anomalies compares well with the two observational data sets. Considering the large uncertainty in observational precipitation at the global scale, the IGSM-CAM simulates reasonable past changes in precipitation.

An analysis of the El Niño–Southern Oscillation (ENSO) in the IGSM is shown in Fig. 11. Figure 11 shows the Nino3.4 index (defined as the average of sea surface temperature anomalies over the region 5° S–5° N and 170° W–120° W) for the IGSM simulation and HadCRUT4 observation and the SSTs regressed upon the Nino3.4 index, along with the monthly standard deviation and the maximum entropy power spectrum of the Nino3.4 index. This analysis reveals that the IGSM produces ENSO variability that occurs on the observed timescale and with a realistic seasonality. However, the amplitudes of the simulated ENSO tend to be larger than observed. The associated SST pattern shows a general agreement with the observations and demonstrates the ability of the IGSM to realistically simulate the meridional extent of the anomalies in the eastern Pacific. As a result, the IGSM-CAM shows a reasonable ENSO variability

in precipitation, cloud cover and wind patterns (not shown). However, like most AOGCMs, the ENSO simulated in the IGSM is too narrowly confined to the Equator and shows characteristics more reminiscent of central-Pacific ENSO types than of eastern-Pacific types (Yu and Kim, 2010).

Altogether, Figs. 9 and 10 demonstrate that the IGSM-CAM framework simulates observed variability in the zonal-mean surface air temperature and precipitation significantly better than the IGSM, especially outside of the tropics. In the tropics, the IGSM benefits from a reasonable simulation of the ENSO, largely driven by the use of observed wind stress to force the 3-D ocean model. This is an important feature of the IGSM-CAM considering that the ENSO can remotely affect regional climate through teleconnections.

5.3 Past and future trends in global and regional climate

Figure 12 shows the historical changes in global mean land-ocean and land-only surface air temperature and global mean precipitation anomalies from the 1901–1950 period for all the IGSM-CAM simulations and for observations. Overall, the global mean surface air temperature and precipitation simulated in the IGSM-CAM show reasonable agreement with the observational record and are consistent with the CMIP5 multi-model ensemble. The land-ocean temperature displays a strong agreement with the CMIP5 models, as it generally overlaps the 25–75 % bounds of the CMIP5 models. After 2000, both the IGSM-CAM ensemble and
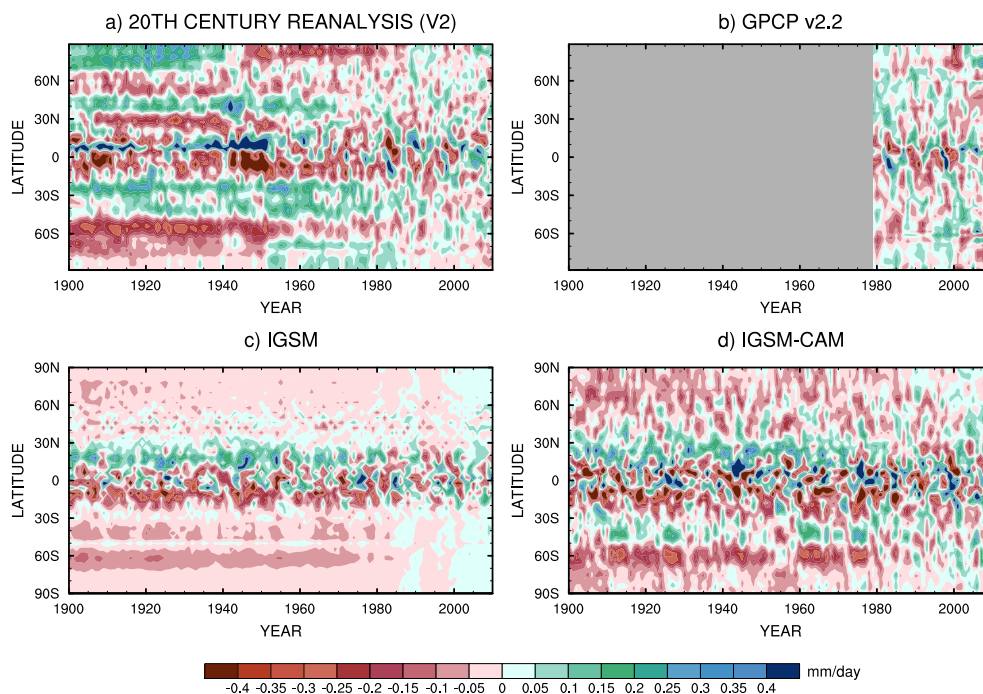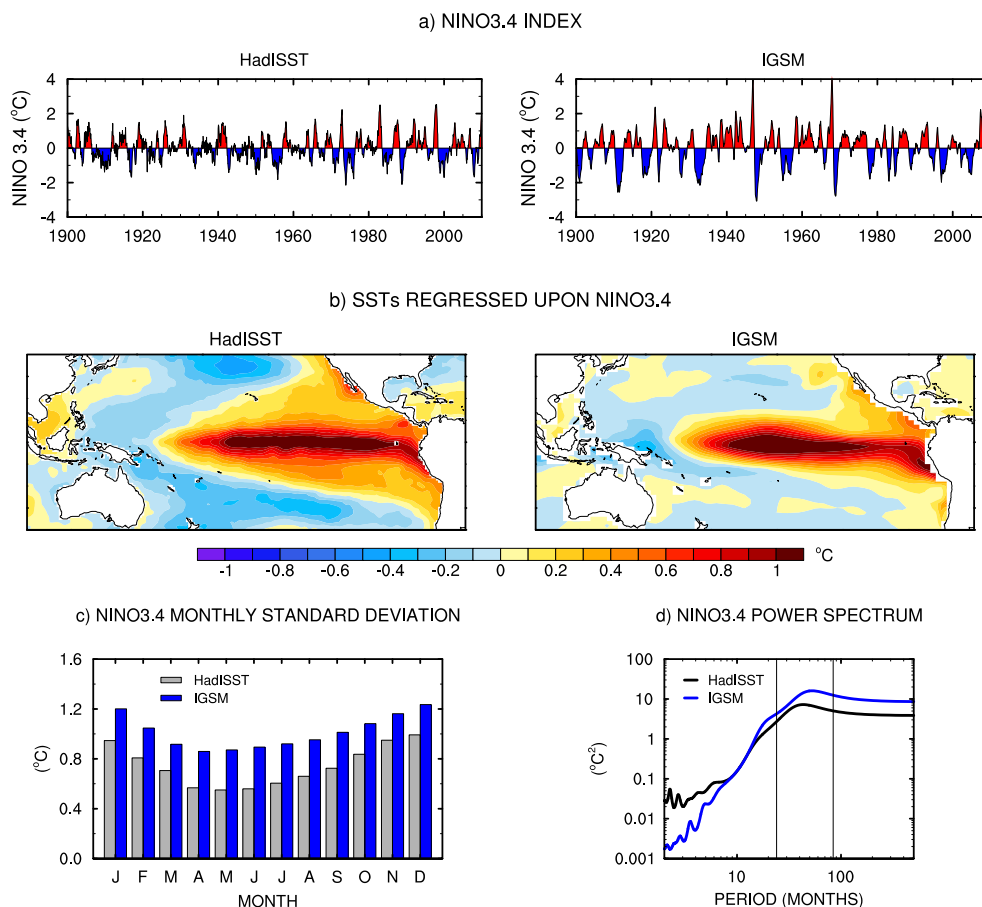
Fig. 10. Hovmöller diagrams of zonal-mean precipitation anomalies from the 1981–2010 mean (mm day^{-1}) for the IGSM and IGSM-CAM simulations, under median climate sensitivity, and for the GPCP v2.2 and 20CR V2.

the CMIP5 models tend to overestimate the global mean land-ocean warming. However, there is good agreement when only land temperature is considered. This indicates that the IGSM-CAM and the CMIP5 models overestimate SST warming. Recent studies suggest that the recent hiatus in surface warming is the result of greater ocean heat uptake by the deep ocean and less by the upper ocean layers (Balmaseda et al., 2013), which is mainly caused by natural variability (Meehl et al., 2013). A potential cause for discrepancies in the global mean temperature after 2000 between the IGSM-CAM simulations and the observations is that the IGSM2.3 version used in the IGSM-CAM simulations has a lower ocean heat uptake rate than most CMIP3 models – although it is unclear how it compares to the CMIP5 models (Forest et al., 2008). In addition, the estimation of the climate parameters used in this study was conducted based on observational data up to 1995. As a result, an updated analysis using data up to 2012 might improve the simulation of the historical surface air temperature changes, including the hiatus of post-2004. The IGSM-CAM simulates past changes in global mean precipitation reasonably well compared to the reconstruction of global mean precipitation, albeit with less year-to-year variability. Before 2000, the IGSM-CAM precipitation anomalies tend to overlap the 25–75 % bounds of the CMIP5 models. After 2000, they tend to be slightly higher than the observations and the 25–75 % bounds of the CMIP5 models but stay mostly within the 5–95 % bounds of the CMIP5 models. The IGSM-CAM simulation of past

global mean precipitation changes are well within the large uncertainty in the observations shown in Smith et al. (2013).

Figure 13 shows past changes and projections of future changes in global mean surface air temperature and global mean precipitation anomalies from the 1901–1950 period for all the IGSM-CAM simulations. The IGSM-CAM simulates a broad range of increases in surface temperature at the last decade of the 21st century, with a global increase between 4.1 and 7.4 °C (3.6 and 7.0 °C from the 1981–2000 mean) for the reference scenario and between 2.1 and 3.9 °C (1.6 and 3.5 °C from the 1981–2000 mean) for the stabilization scenario. Even though the IGSM-CAM simulations rely on only three sets of climate parameters, the range of warming is in excellent agreement with Sokolov et al. (2009), who performed a 400-member ensemble of climate change simulations with the IGSM version 2.2 for the median unconstrained emissions scenario, with Latin Hypercube sampling of climate parameters based on probability density functions estimated by Forest et al. (2008). They found that the 5th and 95th percentiles of the distribution of surface warming for the last decade of the 21st century relative to the 1981–2000 mean are respectively 3.8 and 7.0 °C when only considering climate uncertainty. This confirms that the low and high climate sensitivity simulations presented in this study are representative of, respectively, the 5th and 95th percentiles of the probability distribution of 21st century changes in surface air temperature based on previous work (Sokolov et al., 2009). Furthermore, the IGSM-CAM global

a) NINO3.4 INDEX

b) SSTs REGRESSED UPON NINO3.4

c) NINO3.4 MONTHLY STANDARD DEVIATION

d) NINO3.4 POWER SPECTRUM

Fig. 11. (a) Nino3.4 index, defined as the average of sea surface temperature anomalies over the region 5° S–5° N and 170° W–120° W; **(b)** sea surface temperature regressed upon the Nino3.4 index; **(c)** monthly standard deviation of the Nino3.4 index; and **(d)** maximum entropy power spectrum of the Nino3.4 index for the IGSM, under median climate sensitivity, and for the HadISST over the 1901–2010 period. The vertical lines correspond to periods of 2 and 7 yr.
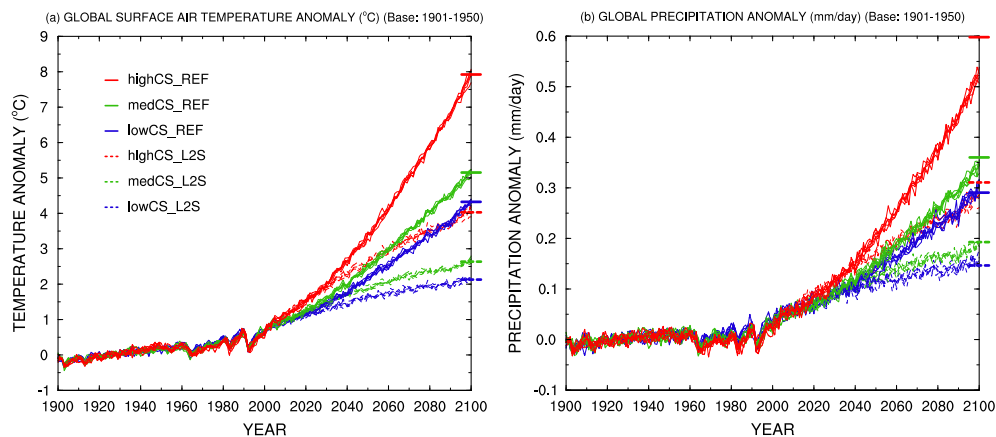
mean surface air temperature anomalies at the end of the simulations (year 2100) are in excellent agreement with simulations of stand-alone IGSM2.3 with the same climate parameters (shown by the horizontal lines in Fig. 13). This demonstrates the consistency in the global climate response within the framework, largely due to the consistent SST forcing and the matching climate parameters in the IGSM and CAM. Meanwhile, the changes in global mean precipitation at the last decade of the 21st century show increases between 0.15 and 0.27 mm day^{-1} for the stabilization scenario and between 0.28 and 0.49 mm day^{-1} for the reference scenario. Even though the IGSM and CAM have very distinct microphysics parameterization schemes, global mean precipitation anomalies in 2100 agree well between the IGSM-CAM and stand-alone IGSM2.3 simulations, except for the high climate sensitivity under the reference scenario where the IGSM-CAM underestimates the increase in precipitation compared to the IGSM. Figure 13 indicates that implementing a 660 ppm CO_2-equivalent stabilization policy can significantly decrease future global warming, with the lower bound

warming (from the 1901–1950 mean) just above 2 °C and the upper bound equal to the lower bound warming of the unconstrained emissions scenario. It also presents evidence that the uncertainty associated with the climate response is of comparable magnitude to the uncertainty associated with the emissions scenarios, thus demonstrating the need to account for both.
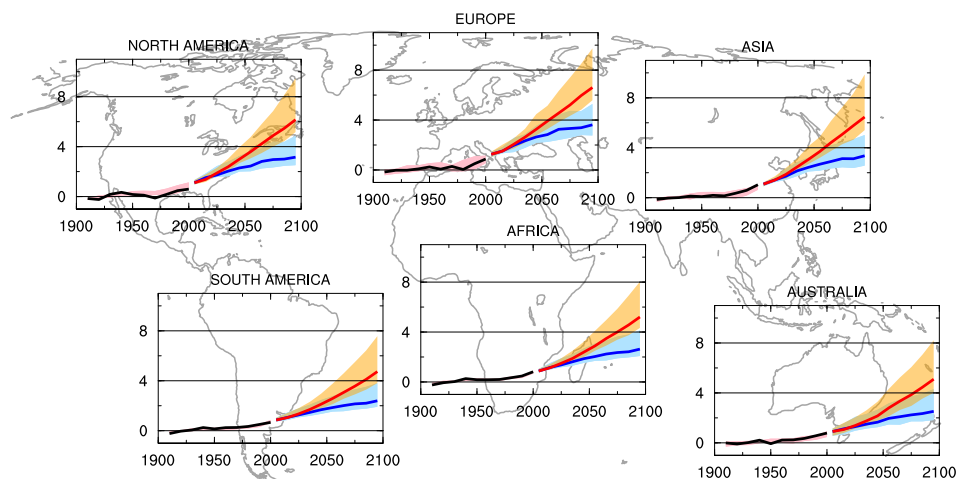
Figure 14 shows the decadal mean continental surface air temperature anomalies from the 1901–1950 mean for the IGSM-CAM simulations (from 1906 to 2100) and for the HadCRUT4 (from 1906 to 2005). Over the historical period, the IGSM-CAM simulates well the observed trends in surface air temperature at the continental scale. This is especially true for South America and Africa where the range of the IGSM-CAM simulations, with different values of climate sensitivity and different initial conditions, is narrow and in very good agreement with the observations. For Europe and North America, the range of the IGSM-CAM simulations is wider, indicating a larger year-to-year variability over these regions. Like the global mean temperature projections, the
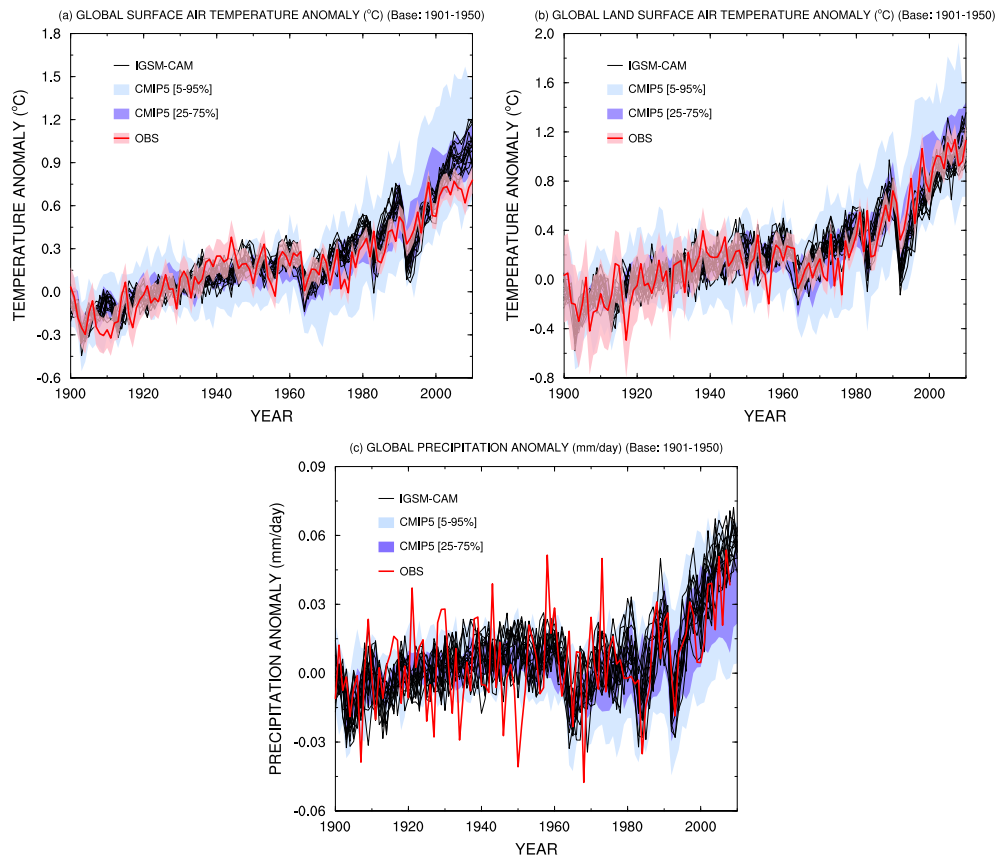
Fig. 12. Global mean **(a)** land-ocean surface air temperature anomalies (°C), **(b)** land-only surface air temperature anomalies and **(c)** precipitation anomalies (mm day^{-1}) from the 1901–1950 mean for the IGSM-CAM simulations, observations and CMIP5 models. The IGSM-CAM simulations are represented by black solid lines. The observations are shown in red lines, with the uncertainty shown in a pink band when available. The 5–95 % (25–75 %) range of the CMIP5 simulations are shown in light (dark) blue. For the land-ocean surface air temperature, HadCRUT4 is shown for observations. For land-only surface air temperature, CRUTEM4 is shown. For precipitation, REC is shown.

Fig. 13. Global mean **(a)** surface air temperature anomalies (°C) and **(b)** precipitation anomalies (mm day^{-1}) from the 1901–1950 mean for the IGSM-CAM simulations. The reference (REF) and stabilization (L2S) scenarios are represented by, respectively, solid and dashed lines. The simulations with a climate sensitivity of 2.0, 2.5 and 4.5 °C are shown respectively in blue, green and red. The thin lines represent each of the five-member ensemble with different initial conditions and random wind sampling while the thick lines represent the ensemble means. The 2100 anomalies from the stand-alone IGSM2.3 simulations with the same climate parameters and emissions scenarios are represented by the horizontal lines on the right y axis.

Fig. 14. Decadal mean continental surface air temperature anomalies (°C) from the 1901–1950 mean for the IGSM-CAM simulations (from 1906 to 2100) and for the HadCRUT4 (from 1906 to 2005). The black lines represent the observations and the pink bands show the range of temperature anomalies among all the historical IGSM-CAM simulations. The blue and orange bands show the range of temperature anomalies for the REF and L2S scenarios among all the IGSM-CAM simulations. The red and blue lines show the mean of the five-member ensemble IGSM-CAM simulations under the median climate sensitivity. From 1906 to 2005, the decadal averages are centered on the decade boundaries, whereas for the future period they are centered on the decade mid-points.

regional projections display a wide range of warming. All continents are projected to warm by at least 2 °C, even under the stabilization scenario, and North America, Europe and Asia are projected to warm more than South America, Africa and Australia. By 2100, the range of warming for the two emissions scenarios separates and does not overlap, except for Australia. This further emphasizes the significant impact of implementing a 660 ppm CO_2-equivalent stabilization policy. Figure 14 demonstrates the IGSM-CAM capability to simulate uncertainty in future warming at the continental scale, like the IPCC AR4 multi-model analysis (see Box 11.1, Fig. 1, Christensen et al., 2007).

5.4 Regional projections

Figure 15 shows maps of the IGSM-CAM ensemble mean changes in annual mean surface air temperature between the 1981–2000 and 2081–2100 periods. Figure 15 further demonstrates the wide range of warming between the different scenarios. It also shows well-known patterns of polar amplification and of stronger warming over land. The warming is significantly weaker over the ocean, except over the coast of Antarctica and over the Arctic Ocean where melting sea-ice leads to a stronger warming. In addition, the IGSM-CAM projects a lack of warming over the ocean south of Greenland, a feature present in many models (Meehl et al., 2007a). Over high-latitude land areas, the warming ranges between 5 and 12 °C for the reference scenario and between 2 and 6 °C for the stabilization scenario. These results indicate that several regions are at risk of severe warming. For example, the high climate sensitivity simulation for the reference scenario shows northern Eurasia warming by as much

as 12 °C in the annual mean and 16 °C in wintertime (not shown). Similarly, western Europe would warm by 8 °C in the annual mean and 12 °C in summertime. To put this in perspective, during the European summer heat wave of 2003, Europe experienced summer surface air temperature anomalies (based on the June-July-August daily averages) reaching up to 5.5 °C with respect to the 1961–1990 mean (Garcia-Herrera et al., 2010). That heat wave resulted in more than 70 000 deaths in 16 countries (Robine et al., 2008). A warming of 12 °C in summertime would likely result in serious strain on the most vulnerable populations and could lead to significant casualties. Figure 16 shows maps of the IGSM-CAM changes in annual mean surface air temperature between the 1981–2000 and 2081–2100 periods for each simulation with different initial conditions under the median climate sensitivity and the stabilization scenario. The different initial conditions lead to visible differences in the magnitude and location of the largest warming. This is particularly clear over the polar regions, like northern Eurasia and Canada, and some differences can also be seen over the contiguous United States and Australia. While these differences are significantly smaller than between simulations with different values of climate sensitivity or emissions scenarios, the differences are large enough to have potentially significant climate impacts.

The same analysis for precipitation is shown in Figs. 17 and 18. Precipitation changes show general patterns that are consistent among all ensemble means. The overall agreement in the patterns of precipitation change is the result of averaging over multiple simulations with different initial conditions, thus extracting the forced signal, and of relying on one single GCM. Figure 17 also shows that the magnitude
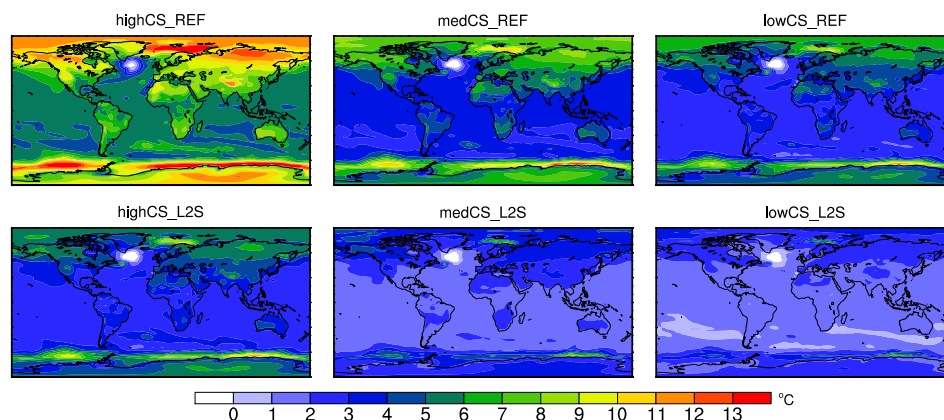
Fig. 15. Changes in annual mean surface air temperature (°C) for the period 2081–2100 relative to 1981–2000 for the five-member ensemble means of the IGSM-CAM simulations.
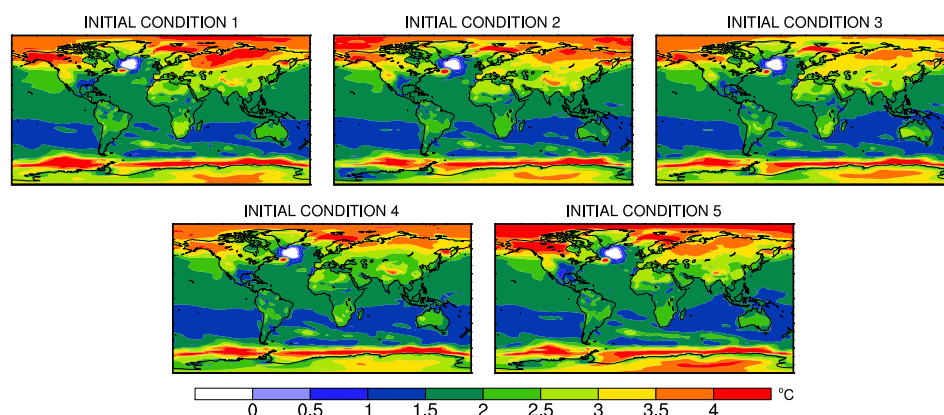
Fig. 16. Changes in annual mean surface air temperature (°C) for the period 2081–2100 relative to 1981–2000 for the five simulations with different initial conditions under the median climate sensitivity and L2S scenario.

of precipitation changes generally increases with increasing warming so that the high climate sensitivity simulation for the reference scenario presents the largest overall precipitation changes. Precipitation tends to increase over most of the tropics, at high latitudes and over most land areas. In contrast, the subtropics and mid-latitudes experience decreases in precipitation over the ocean. Decreases in precipitation over Europe (except northern Europe), northwest Africa, southeast Africa and Patagonia agree well with the results from the IPCC AR4 (Meehl et al., 2007a, see Fig. 10.12). Decreases in precipitation over the Western United States are similar to the projections with CCSM3. Nevertheless, there is also regional uncertainty associated with differences in the climate sensitivity (Sokolov and Monier, 2012). Modest decreases in rainfall in southwestern Australia are present in most of the IGSM-CAM simulations but not all, and they are not as marked as in the IPCC AR4. Several regions even exhibit changes in precipitation of different signs among all the simulations. That is the case of Australia, southeast China and India. These regions tend to experience decreases in precipitation for the simulations with the least warming but increases in precipitation for the simulations with the strongest warming. While the ensemble mean simulations with different climate parameters and emissions scenarios tend to show consistent patterns of precipitation change, the large impact of the initial conditions can be seen in Fig. 18. Perturbing the initial conditions leads to regional differences, both in the magnitude and in the sign of the precipitation changes. For example, over the Eastern United States and northern Eurasia, the increase in precipitation shows different magnitude and location of the maxima. Meanwhile, regions like the Western United States, Australia or India exhibit drying to different extents in the simulations with different initial conditions. This result suggests that natural variability is larger in these regions than anthropogenically driven changes in precipitation.

Figure 19 shows the median and the range of surface air temperature changes over the globe, each hemisphere and the seven continents for the period 2081–2100 relative to 1981–2000 for the IGSM-CAM under the reference
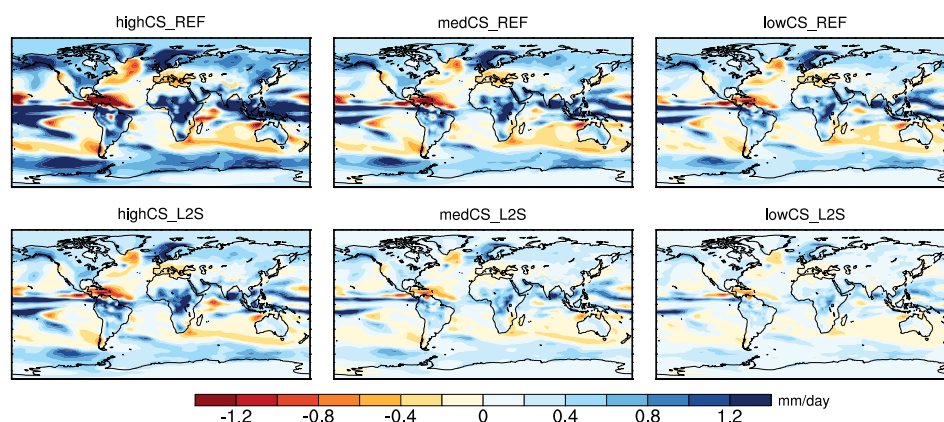
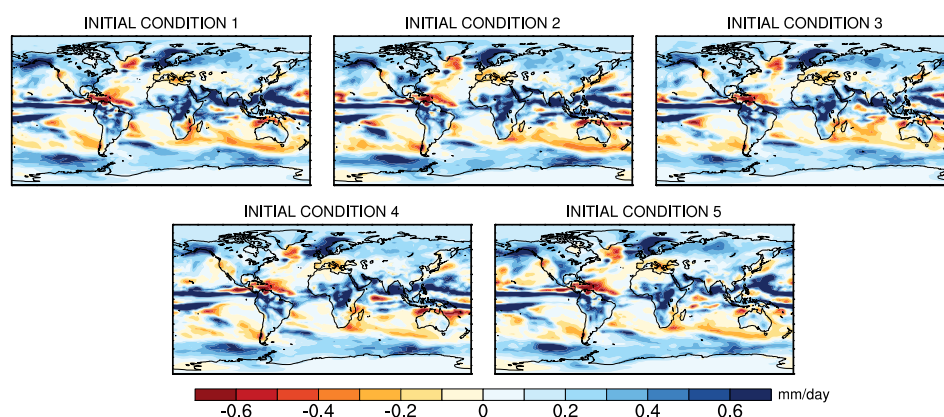**Fig. 17.** Same as Fig. 15 but for changes in precipitation (mm day^{-1}).

Fig. 18. Same as Fig. 16 but for changes in precipitation (mm day^{-1}).

and stabilization scenarios and for the CMIP5 models under the RCP8.5 and RCP4.5. For the IGSM-CAM, the range is estimated as the minimum and maximum changes over the 30 simulations, while the median is estimated as the ensemble mean for the median climate sensitivity. For the CMIP5 models, the range is estimated as the 90 % range amongst all the models (by removing the "outliers"), and the median is calculated based on all 31 models. Figure 19 shows generally good agreement in the range of projected changes between the IGSM-CAM and the CMIP5 models, except over Antarctica where the IGSM-CAM overestimates the warming. Nonetheless, the IGSM-CAM tends to slightly overestimate the warming compared to the CMIP5 models, which can be explained by the differences in emissions scenarios, the two scenarios used in this study having slightly larger radiative forcing than the RCP8.5 and RCP4.5 used by the CMIP5 models. Figure 19 further confirms the wide range of uncertainty in the future global and regional climate change associated with both the uncertainty in emissions and the climate response. Under the unconstrained emissions scenario, every continent is projected to warm by at least 2.5 °C. Meanwhile, the implementation of the

stabilization policy examined in this study leads to a significant reduction in warming over all continents. Generally, the upper bound warming under the stabilization scenario and the lower bound warming under the reference scenario agree well.

Figure 20 shows the same analysis as in Fig. 19 for precipitation. Changes in precipitation at the continental scale display a large uncertainty in both the IGSM-CAM and CMIP5 ensemble simulations. Although the range of precipitation changes does not always overlap, the size of the range is generally in good agreement. Unlike the CMIP5 ensemble, where some models project decreases in precipitation over several continents, i.e. Africa, South America and Australia and Oceania, the IGSM-CAM simulates increases in precipitation over all the continents. This leads to a general overestimation of precipitation increases in the IGSM-CAM simulations compared to the CMIP5 models. The agreement between the two ensemble simulations varies widely between the different continents and is much stronger for the Northern Hemisphere than for the Southern Hemisphere. The two ensemble simulations show good agreement over Europe and Asia. Over Australia and Oceania, the IGSM-CAM simulates
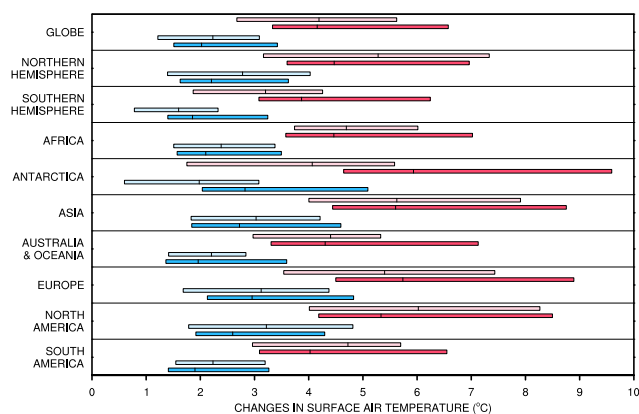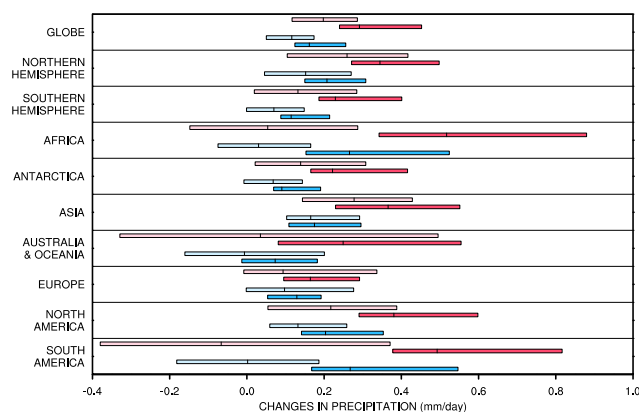
Fig. 19. Range of and median surface air temperature changes (°C) over the globe, each hemisphere and the seven continents for the period 2081–2100 relative to 1981–2000 simulated by the IGSM-CAM under the reference and level 2 stabilization scenarios and by 31 CMIP5 models under the RCP8.5 and RCP4.5. The reference scenario is shown in dark (light) red for the IGSM-CAM (CMIP5 models) and the stabilization scenario is shown in dark (light) blue for the IGSM-CAM (CMIP5 models). For the IGSM-CAM, the range is estimated as the minimum and maximum changes over the 30 simulations, while the median is estimated as the ensemble mean for the median climate sensitivity. For the CMIP5 models, the range is estimated as the 90 % range amongst all the models (by removing the "outliers"), and the median is calculated based on all 31 models.

Fig. 20. Same as Fig. 19 but for changes in precipitation (mm day^{-1}).

a similar range of precipitation increase but fails to simulate the decrease in precipitation displayed by several CMIP5 models. Finally, the ranges of precipitation changes over Africa and South America do not overlap, but display similar size. Africa and South America are arguably the two continents where the CMIP3 models show the least agreement in the sign of precipitation changes and where CCSM3 is an outlier (see the Supplement from Christensen et al., 2007).

6 Discussion and conclusion

This paper describes a new framework where the MIT IGSM, an integrated assessment model that couples an Earth system model of intermediate complexity to a human activity model, is linked to the three-dimensional atmospheric model CAM version 3. Although it is not a state-of-the-art fully coupled GCM, the IGSM-CAM modeling system is an efficient and flexible framework to explore uncertainties in the future global and regional climate change. First, the IGSM-CAM incorporates a human activity model, thus it can be used to examine uncertainties in emissions resulting from both uncertainties in the underlying socio-economic characteristics of the economic model and in the choice of climate-related policies. Second, the key climate parameters controlling the climate response (climate sensitivity, strength of aerosol forcing and ocean heat uptake rate) can be consistently changed within the modeling framework, so that the

IGSM-CAM can be used to address uncertainty in the climate response to future changes in greenhouse gases and aerosols concentrations. As a result, the IGSM-CAM can make use of the IGSM probabilistic ensemble projections and can then subsample them at key quantile values (e.g., 5th and 95th percentile, median) to obtain a first-order assessment of regional uncertainties without necessarily having to run the entire set of members (in the order of several hundred simulations) from the IGSM ensemble. In addition, since the atmospheric chemistry and the land and ocean biogeochemical cycles are computed within the IGSM 2-D zonal-mean atmosphere, the IGSM-CAM is more computationally efficient than a fully coupled GCM, like CCSM3.

The IGSM-CAM is evaluated against several observational data sets and compared to the CMIP3 models. The IGSM-CAM provides significant improvements over the IGSM in the simulation of present-day mean temperature, precipitation and moisture fields, as well as past trends and natural variability. This is not entirely surprising considering that the IGSM includes an Earth system model of intermediate complexity with a 2-D zonal-mean atmosphere. Even though the IGSM 2-D atmosphere includes parameterizations of heat, moisture, and momentum transports by large-scale eddies, it cannot accurately simulate the ocean/land contrasts and atmospheric circulations. For this reason, linking the IGSM to a 3-D atmospheric model shows substantial improvements. The IGSM-CAM not only realistically simulates the present-day mean climate and past variability but it also reproduces ENSO variability with realistic time scales, seasonality and patterns of SST anomalies, albeit with stronger magnitudes than observed. Finally, the IGSM-CAM shares the same general strengths and limitations as current climate models in simulating observed changes in surface temperature and precipitation, as well as in the present-day mean climate. The IGSM-CAM model error in surface temperature and precipitation over land are very similar to CCSM3, which shares the same atmospheric model. This

indicates that the two modeling systems share biases and that model errors within CAM are likely to propagate in IGSM-CAM climate projections. If the IGSM were linked to a different 3-D atmospheric model, it would likely lead to different textures in the model biases and errors and propagate into the range of projections.

The IGSM-CAM was also used to simulate future climate change under two emissions scenarios and three sets of climate parameters. The two emissions scenarios tested are a reference scenario with unconstrained emissions, similar to the RCP8.5 scenario, and a stabilization scenario at 660 ppm CO_2-equivalent by 2100, similar to the RCP4.5 scenario. The three values of climate sensitivity were chosen to provide a good approximation for the median, and the 5th and 95th percentiles of the probability distribution of 21st century changes in surface air temperature from Sokolov et al. (2009). Results show a wide range of future warming and changes in precipitation at the global and regional scales. The implementation of a stabilization scenario significantly decreases the projected climate warming. Over each continent, the upper bound climate warming under the stabilization scenario is comparable with the lower bound increase in temperature in the reference scenario. This underscores the effectiveness of a global climate policy, even given the uncertainty in the climate response. This also demonstrates the need to account for both sources of uncertainty in climate change projections. Changes in surface air temperature and precipitation for the different values of climate sensitivity and the different emissions scenarios generally show similar patterns of change, but with different magnitude, once they are averaged over multiple simulations with different initial conditions. However, simulations with different initial conditions display visible differences in both magnitude and location of the largest warming and, for precipitation, in the sign of the changes. This underlines the importance of natural variability in projections of regional climate change, a finding that is in agreement with other studies (Hawkins, 2011; Deser et al., 2012a, b).

The fact that the patterns of change for the ensemble mean is similar for different values of climate sensitivity is due to the fact that the IGSM-CAM framework relies on a single atmospheric model and also on the cloud radiative adjustment method used to change the climate sensitivity of the model. Unlike the more traditional perturbed physics approach, which can produce several versions of a model with the same climate sensitivity but with very different regional patterns of change, the cloud radiative adjustment method can only produce one version of the model, with one specific value of climate sensitivity (Sokolov and Monier, 2012). As a result, the IGSM-CAM cannot cover the full uncertainty in regional patterns of climate change. Nonetheless, the IGSM-CAM framework has some advantages over the perturbed physics approach. The perturbed physics approach has been implemented in several AOGCMs to obtain versions of a model with different values of climate sensitivity

(Murphy et al., 2004; Stainforth et al., 2005; M. Collins et al., 2006; Yokohata et al., 2010; Sokolov and Monier, 2012). In most cases, the obtained climate sensitivities do not cover the full range of uncertainty based on the observed 20th century climate change and they tend to cluster around the climate sensitivity of the unperturbed version of the given model (Sokolov and Monier, 2012). Typically, in a perturbed physics ensemble, each version of the model with a different perturbation is weighted equally regardless of the obtained climate sensitivity, even though the values of climate sensitivity are not equally probable. In comparison, any value of climate sensitivity within the wide range of uncertainty can be obtained in the IGSM-CAM framework, which allows Monte Carlo type probabilistic climate projections to be conducted where values of uncertain parameters not only cover the whole uncertainty range, but also cover their probability distribution homogeneously.

The IGSM-CAM simulations of future climate change were also compared to simulations from 31 CMIP5 models under the RCP4.5 and RCP8.5 scenarios. Even though it uses only one single model, the IGSM-CAM simulates a range of future warming at the continental scale that is in very good agreement with the range from the CMIP5 models, except over Antarctica, where the IGSM-CAM significantly overestimates the warming. This demonstrates that, by sampling the climate system response, one single climate model can essentially reproduce the range of future continental warming simulated by more than 30 different models. It also suggests that the range of warming obtained by the CMIP5 models is likely driven by the range of the models' climate sensitivity, which is similar to that of the IGSM distribution (Andrews et al., 2012). For precipitation, the IGSM-CAM also simulates a range of continental changes of comparable size as the CMIP5 models. The ranges of precipitation projected in both ensemble simulations show good agreement over Asia and Europe. However, they do not overlap (but display similar sizes) for Africa and South America, two continents where models generally show little agreement in the sign of precipitation changes and where CCSM3 tends to be an outlier. A particular difference between the two ensemble simulations is that the IGSM-CAM simulations with the largest warming are usually associated with the largest increase in precipitation. That is due to the linear relationship between changes in temperature and precipitation within a particular model (Senior and Mitchell, 1993; Sokolov et al., 2003). On the other hand, considering multiple models like the CMIP5, it is possible to have a model that simulates large warming with little changes in precipitation and another model that simulates little warming with large changes in precipitation.

An agreement between the IGSM-CAM and the CMIP5 models is neither guaranteed nor necessary, since the IGSM-CAM constitutes a different modeling framework, with an additional human component and thus different forcing. The results mainly underline the fact that structural uncertainty cannot be generalized as the largest or sole source of

uncertainty in climate projections and that the IGSM-CAM accounts for other important sources of uncertainty. Multi-model ensemble simulations that do not sample the climate system response in each climate model likely underestimate the possible range of future climate change. At the same time, the IGSM-CAM framework also cannot cover the full range of uncertainty in future climate change because it only relies on one particular climate model. Structural uncertainty has been investigated with the IGSM using a pattern scaling method based on the regional patterns of climate change from the various IPCC AR4 models (Schlosser et al., 2013; Monier et al., 2013a, b). Yet, the IGSM-CAM has significant advantages over pattern scaling methods, including the capability to simulate regional climate variability and its past and future changes, to study changes in variables that do not scale well using this method (such as wind vectors and other dynamical quantities) and to simulate changes in extreme events (Monier and Gao, 2013). Together with the pattern scaling method, the IGSM-CAM framework has been used to investigate the role of various sources of uncertainty on future climate projections over the United States (Monier et al., 2013a) and northern Eurasia (Monier et al., 2013b).

While this paper provides useful information on bounds of probable climate change at the continental and regional scales, ensemble simulations are necessary to obtain probability distribution of future changes. In future work, the IGSM2.3 will be used to perform Monte Carlo simulations, with Latin Hypercube sampling of uncertain climate parameters, resulting in a large ensemble in the order of several hundred members. This will provide probabilistic projections of climate change over the 21st century. It will then be possible to run ensemble simulations of the IGSM-CAM based on a sub-sampling of the probabilistic projections of global surface air temperature changes by the end of the 21st century. As such, probabilistic projections of regional climate change could be obtained with a smaller number of ensemble members than usually needed for Monte Carlo simulation, e.g., 20 simulations representing every 20 quantiles of the IGSM probabilistic distribution of global mean surface temperature changes. In addition, further work is required to investigate aspects of climate change other than changes in the mean state. For example, changes in the frequency and magnitude of extreme events, such as heat waves or storms, are of primary importance for impact studies and to inform policy-makers. For this reason, the IGSM-CAM framework will be utilized for a wide range of applications on continental and regional climate change and their societal impacts.

7   Code availability

The source code of the IGSM-CAM can be obtained upon request (see http://globalchange.mit.edu/research/IGSM/download). The code is released on an "as is" basis, which means that a third party may face problems compiling and running the code on a platform that differs significantly from the MIT Joint Program's high-performance computing cluster. Unfortunately, the MIT Joint Program does not have resources available at this time to provide technical support but we are currently working on improving the usability of the modeling framework.

Supplementary material related to this article is available online at http://www.geosci-model-dev.net/6/2063/2013/gmd-6-2063-2013-supplement.pdf.

References

Adler, R. F., Huffman, G. J., Chang, A., Ferraro, R., Xie, P.-P., Janowiak, J., Rudolf, B., Schneider, U., Curtis, S., Bolvin, D., Gruber, A., Susskind, J., and Arkin, P.: The version-2 global precipitation climatology project (GPCP) monthly precipitation analysis (1979–present), J. Hydrometeorol., 4, 1147–1167, doi:10.1175/1525-7541(2003)004<1147:TVGPCP>2.0.CO;2, 2003.

Andrews, T., Gregory, J., Webb, M., and Taylor, K.: Forcing, feedbacks and climate sensitivity in CMIP5 coupled atmosphere-ocean climate models, Geophys. Res. Lett., 39, L09712, doi:10.1029/2012GL051607, 2012.

Annan, J. D. and Hargreaves, J. C.: Understanding the CMIP3 Multimodel Ensemble, J. Climate, 24, 4529–4538, doi:10.1175/2011JCLI3873.1, 2011.

Balmaseda, M. A., Trenberth, K. E., and Källén, E.: Distinctive climate signals in reanalysis of global ocean heat content, Geophys. Res. Lett., 40, 1754–1759, doi:10.1002/grl.50382, 2013.

Brovkin, V., Claussen, M., Driesschaert, E., Fichefet, T., Kick-lighter, D., Loutre, M., Matthews, H., Ramankutty, N., Scha-effer, M., and Sokolov, A.: Biogeophysical effects of histori-cal land cover changes simulated by six Earth system mod-els of intermediate complexity, Clim. Dynam., 26, 587–600, doi:10.1007/s00382-005-0092-6, 2006.

Christensen, J. H., Hewitson, B., Busuioc, A., Chen, A., Gao, X., Held, R., Jones, R., Kolli, R. K., Kwon, W.-T., Laprise, R., Mag-aña Rueda, V., Mearns, L., Menéndez, C. G., Räisänen, J., Rinke, A., Sarr, A., and Whetton, P.: Regional climate projections, in: Climate Change 2007: The Physical Science Basis, Contribution of Working Group I to the Fourth Assessment Report of the In-tergovernmental Panel on Climate Change, edited by: Solomon, S., Qin, D., Manning, M., Chen, Z., Marquis, M., Averyt, K. B., Tignor, M., and Miller, H. L., Cambridge University Press, Cam-bridge, United Kingdom and New York, NY, USA, 2007.

Clarke, L., Edmonds, J., Jacoby, H., Pitcher, H., Reilly, J., and Richels, R.: Scenarios of greenhouse gas emissions and atmo-spheric concentrations, Sub-report 2.1A of Synthesis and As-sessment Product 2.1 by the US Climate Change Science Pro-gram and the Subcommittee on Global Change Research, De-partment of Energy, Office of Biological & Environmental Re-search, Washington, DC, 2007.

Collins, M., Booth, B. B. B., Harris, G. R., Murphy, J. M., Sex-ton, D. M. H., and Webb, M. J.: Towards quantifying uncer-tainty in transient climate change, Clim. Dynam., 27, 127–147, doi:10.1007/s00382-006-0121-0, 2006.

Collins, W. D., Rasch, P. J., Boville, B. A., Hack, J. J., McCaa, J. R., Williamson, D. L., Kiehl, J. T., Briegleb, B., Bitz, C., Lin, S. J., Zhang, M., and Dai, Y.: Description of the NCAR Community Atmosphere Model (CAM 3.0), Ncar/tn-464+str, NCAR Techni-cal Note, 2004.

Collins, W. D., Bitz, C. M., Blackmon, M. L., Bonan, G. B., Bretherton, C. S., Carton, J. A., Chang, P., Doney, S. C., Hack, J. J., Henderson, T. B., Kiehl, J. T., Large, W. G., McKenna, D. S., Santer, B. D., and Smith, R. D.: The Community Climate System Model version 3 (CCSM3), J. Climate, 19, 2122–2143, doi:10.1175/JCLI3761.1, 2006.

Compo, G. P., Whitaker, J. S., Sardeshmukh, P. D., Matsui, N., Al-lan, R. J., Yin, X., Gleason, B. E., Vose, R. S., Rutledge, G., Bessemoulin, P., Brönnimann, S., Brunet, M., Crouthamel, R. I., Grant, A. N., Groisman, P. Y., Jones, P. D., Kruk, M., Kruger, A. C., Marshall, G. J., Maugeri, M., Mok, H. Y., Nordli, Ø., Ross, T. F., Trigo, R. M., Wang, X. L., Woodruff, S. D., and Worley, S. J.: The Twentieth Century Reanalysis Project, Q. J. Roy. Meteorol. Soc., 137, 1–28, doi:10.1002/qj.776, 2011.

Dalan, F., Stone, P. H., and Sokolov, A. P.: Sensitivity of the ocean's climate to diapycnal diffusivity in an EMIC. Part II: Global warming scenario, J. Climate, 18, 2482–2496, doi:10.1175/JCLI3412.1, 2005.

Dee, D. P., Uppala, S. M., Simmons, A. J., Berrisford, P., Poli, P., Kobayashi, S., Andrae, U., Balmaseda, M. A., Balsamo, G., Bauer, P., Bechtold, P., Beljaars, A. C. M., van de Berg, L., Bid-lot, J., Bormann, N., Delsol, C., Dragani, R., Fuentes, M., Geer, A. J., Haimberger, L., Healy, S. B., Hersbach, H., Hólm, E. V., Isaksen, L., Kållberg, P., Köhler, M., Matricardi, M., McNally, A. P., Monge-Sanz, B. M., Morcrette, J.-J., Park, B.-K., Peubey, C., de Rosnay, P., Tavolato, C., Thépaut, J.-N., and Vitart, F.: The ERA-Interim reanalysis: Configuration and performance of the

data assimilation system, Q. J. Roy. Meteorol. Soc., 137, 553–597, doi:10.1002/qj.828, 2011.

Deser, C., Knutti, R., Solomon, S., and Phillips, A. S.: Communication of the role of natural variability in future North American climate, Nat. Clim. Change, 2, 775–779, doi:10.1038/nclimate1562, 2012a.

Deser, C., Phillips, A., Bourdette, V., and Teng, H.: Uncertainty in climate change projections: the role of internal variability, Clim. Dynam., 38, 527–546, doi:10.1007/s00382-010-0977-x, 2012b.

Dickinson, R. E., Oleson, K. W., Bonan, G., Hoffman, F., Thornton, P., Vertenstein, M., Yang, Z.-L., and Zeng, X.: The Community Land Model and its climate statistics as a component of the Com-munity Climate System Model, J. Climate, 19, 2302–2324, 2006.

Dutkiewicz, S., Sokolov, A. P., Scott, J., and Stone, P. H.: A Three-Dimensional Ocean-Seaice-Carbon Cycle Model and its Coupling to a Two-Dimensional Atmospheric Model: Uses in Climate Change Studies, MIT JPSPGC Report 122, May, 47 pp., available at: http://globalchange.mit.edu/files/document/MITJPSPGC_Rpt122.pdf, 2005.

Dutkiewicz, S., Follows, M. J., and Bragg, J. G.: Modeling the coupling of ocean ecology and biogeochemistry, Global Bio-geochem. Cy., 23, GB4017, doi:10.1029/2008GB003405, 2009.

Eby, M., Weaver, A. J., Alexander, K., Zickfeld, K., Abe-Ouchi, A., Cimatoribus, A. A., Crespin, E., Drijfhout, S. S., Edwards, N. R., Eliseev, A. V., Feulner, G., Fichefet, T., Forest, C. E., Goosse, H., Holden, P. B., Joos, F., Kawamiya, M., Kicklighter, D., Kienert, H., Matsumoto, K., Mokhov, I. I., Monier, E., Olsen, S. M., Ped-ersen, J. O. P., Perrette, M., Philippon-Berthier, G., Ridgwell, A., Schlosser, A., Schneider von Deimling, T., Shaffer, G., Smith, R. S., Spahni, R., Sokolov, A. P., Steinacher, M., Tachiiri, K., Tokos, K., Yoshimori, M., Zeng, N., and Zhao, F.: Historical and ide-alized climate model experiments: an intercomparison of Earth system models of intermediate complexity, Clim. Past, 9, 1111–1140, doi:10.5194/cp-9-1111-2013, 2013.

Forest, C. E., Allen, M. R., Sokolov, A. P., and Stone, P. H.: Constraining climate model properties using optimal fingerprint detection methods, Clim. Dynam., 18, 277–295, doi:10.1007/s003820100175, 2001.

Forest, C. E., Stone, P. H., and Sokolov, A. P.: Constraining climate model parameters from observed 20th century changes, Tellus, 60A, 911–920, doi:10.1111/j.1600-0870.2008.00346.x, 2008.

Garcia-Herrera, R., Diaz, J., Trigo, R. M., Luterbacher, J., and Fischer, E. M.: A Review of the European Summer Heat Wave of 2003, Crit. Rev. Environ. Sci. Technol., 40, 267–306, doi:10.1080/10643380802238137, 2010.

Gleckler, P. J., Taylor, K. E., and Doutriaux, C.: Performance metrics for climate models, J. Geophys. Res., 113, D06104, doi:10.1029/2007JD008972, 2008.

Gregory, J. M., Dixon, K. W., Stouffer, R. J., Weaver, A. J., Driess-chaert, E., Eby, M., Fichefet, T., Hasumi, H., Hu, A., Jung-claus, J. H., Kamenkovich, I. V., Levermann, A., Montoya, M., Murakami, S., Nawrath, S., Oka, A., Sokolov, A. P., and Thorpe, R. B.: A model intercomparison of changes in the At-lantic thermohaline circulation in response to increasing atmo-spheric CO_2 concentration, Geophys. Res. Lett., 32, L12703, doi:10.1029/2005GL023209, 2005.

Hansen, J., Russell, G., Rind, D., Stone, P., Lacis, A., and Lebedeff, S., Ruedy, R., and Travis, L.: Efficient Three-Dimensional Global Models for Climate Studies: Models I

and II, Mon. Weather Rev., 111, 609–662, doi:10.1175/1520-0493(1983)111<0609:ETDGMF>2.0.CO;2, 1983.

Hawkins, E.: Our evolving climate: communicating the effects of climate variability, Weather, 66, 175–179, 2011.

Hegerl, G. C., Zwiers, F. W., Braconnot, P., Gillett, N. P., Luo, Y., Marengo Orsini, J. A., Nicholls, N., Penner, J. E., and Stott, P. A.: Understanding and Attributing Climate Change, in: Climate Change 2007: The Physical Science Basis, Contribution of Working Group I to the Fourth Assessment Report of the Intergovernmental Panel on Climate Change, edited by: Solomon, S., Qin, D., Manning, M., Chen, Z., Marquis, M., Averyt, K. B., Tignor, M., and Miller, H. L., Cambridge University Press, Cambridge, United Kingdom and New York, USA, 2007.

Horowitz, L. W., Walters, S., Mauzerall, D. L., Emmons, L. K., Rasch, P. J., Granier, C., Tie, X., Lamarque, J.-F., Schultz, M. G., Tyndall, G. S., Orlando, J. J., and Brasseur, G. P.: A global simulation of tropospheric ozone and related tracers: Description and evaluation of MOZART, version 2, J. Geophys. Res., 108, 4784, doi:10.1029/2002JD002853, 2003.

Hurrell, J., Hack, J., Phillips, A., Caron, J., and Yin, J.: The dynamical simulation of the Community Atmosphere Model version 3 (CAM3), J. Climate, 19, 2162–2183, doi:10.1175/JCLI3762.1, 2006.

Hurrell, J. W., Hack, J. J., Shea, D., Caron, J. M., and Rosinski, J.: A new sea surface temperature and sea ice boundary dataset for the Community Atmosphere Model, J. Climate, 21, 5145–5153, doi:10.1175/2008JCLI2292.1, 2008.

Jones, P., Lister, D., Osborn, T., Harpham, C., Salmon, M., and Morice, C.: Hemispheric and large-scale land-surface air temperature variations: An extensive revision and an update to 2010, J. Geophys. Res., 117, D05127, doi:10.1029/2011JD017139, 2012.

Jones, P. D., New, M., Parker, D. E., Martin, S., and Rigor, I. G.: Surface air temperature and its changes over the past 150 years, Rev. Geophys., 37, 173–199, doi:10.1029/1999RG900002, 1999.

Kalnay, E., Kanamitsu, M., Kistler, R., Collins, W., Deaven, D., Gandin, L., Iredell, M., Saha, S., White, G., Woollen, J., Zhu, Y., Chelliah, M., Ebisuzaki, W., Higgins, W., Janowiak, J., Mo, K. C., Ropelewski, C., Wang, J., Leetmaa, A., Reynolds, R., Jenne, R., and Joseph, D.: The NCEP/NCAR 40-year reanalysis project, B. Am. Meteorol. Soc., 77, 437–471, doi:10.1175/1520-0477(1996)077<0437:TNYRP>2.0.CO;2, 1996.

Liu, Y.: Modeling the emissions of nitrous oxide (N_2O) and methane (CH_4) from the terrestrial biosphere to the atmosphere, Ph.D. Thesis, Massachusetts Institute of Technology, Earth, Atmospheric and Planetary Sciences Department, Cambridge, MA, ; see also MIT JPSPGC Report 10, available at: http://globalchange.mit.edu/files/document/MITJPSPGC_Rpt10.pdf (last access: 29 November 2013), 1996.

Marshall, J., Hill, C., Perelman, L., and Adcroft, A.: Hydrostatic, quasi-hydrostatic, and nonhydrostatic ocean modeling, J. Geophys. Res., 102, 5733–5752, doi:10.1029/96JC02776, 1997.

Mayer, M., Wang, C., Webster, M., and Prinn, R. G.: Linking local air pollution to global chemistry and climate, J. Geophys. Res., 105, 22869–22896, doi:10.1029/2000JD900307, 2000.

Meehl, G., Stocker, T., Collins, W., Friedlingstein, P., Gaye, A., Gregory, J., Kitoh, A., Knutti, R., Murphy, J., Noda, A., Raper, S., Watterson, I., Weaver, A., and Zhao, Z.-C.: Global Climate Projections, in: Climate Change 2007: The Physical Science Basis, Contribution of Working Group I to the Fourth Assessment Report of the Intergovernmental Panel on Climate Change, edited by: Solomon, S., Qin, D., Manning, M., Chen, Z., Marquis, M., Averyt, K. B., Tignor, M., and Miller, H. L., Cambridge University Press, Cambridge, United Kingdom and New York, NY, USA, 2007a.

Meehl, G. A., Covey, C., Taylor, K. E., Delworth, T., Stouffer, R. J., Latif, M., McAvaney, B., and Mitchell, J. F.: The WCRP CMIP3 multimodel dataset: A new era in climate change research, B. Am. Meteorol. Soc., 88, 1383–1394, 2007b.

Meehl, G. A., Hu, A., Arblaster, J., Fasullo, J., and Trenberth, K. E.: Externally forced and internally generated decadal climate variability associated with the Interdecadal Pacific Oscillation, J. Climate, 26, 7298–7310, doi:10.1175/JCLI-D-12-00548.1, 2013.

Melillo, J., McGuire, A., Kicklighter, D., Moore, B., Vorosmarty, C., and Schloss, A.: Global climate change and terrestrial net primary production, Nature, 363, 234–240, doi:10.1038/363234a0, 1993.

Monier, E. and Gao, X.: Climate change impacts on extreme events in the United States: an uncertainty analysis, Climatic Change, in review, 2013.

Monier, E., Gao, X., Scott, J., Sokolov, A., and Schlosser, C. A.: A framework for modeling uncertainty in regional climate change, Climatic Change, in review, 2013a.

Monier, E., Sokolov, A., Scott, J., Schlosser, C. A., and Gao, X.: Probabilistic projections of 21st century climate change over Northern Eurasia, Environ. Res. Lett., 8, 045008, doi:10.1088/1748-9326/8/4/045008, 2013b.

Morice, C. P., Kennedy, J. J., Rayner, N. A., and Jones, P. D.: Quantifying uncertainties in global and regional temperature change using an ensemble of observational estimates: The HadCRUT4 data set, J. Geophys. Res., 117, D08101, doi:10.1029/2011JD017187, 2012.

Moss, R. H., Edmonds, J. A., Hibbard, K. A., Manning, M. R., Rose, S. K., van Vuuren, D. P., Carter, T. R., Emori, S., Kainuma, M., Kram, T., Meehl, G. A., Mitchell, J. F. B., Nakicenovic, N., Riahi, K., Smith, S. J., Stouffer, R. J., Thomson, A. M., Weyant, J. P., and Wilbanks, T. J.: The next generation of scenarios for climate change research and assessment, Nature, 463, 747–756, doi:10.1038/nature08823, 2010.

Murphy, J. M., Sexton, D. M. H., Barnett, D. N., Jones, G. S., Webb, M. J., and Collins, M.: Quantification of modelling uncertainties in a large ensemble of climate change simulations, Nature, 430, 768–772, doi:10.1038/nature02771, 2004.

Nakicenovic, N., Alcamo, J., Davis, G., de Vries, B., Fenhann, J., Gaffin, S., Gregory, K., Grubler, A., Jung, T. Y., Kram, T., La Rovere, E. L., Michaelis, L., Mori, S., Morita, T., Pepper, W., Pitcher, H. M., Price, L., Riahi, K., Roehrl, A., Rogner, H.-H., Sankovski, A., Schlesinger, M., Shukla, P., Smith, S. J., Swart, R., van Rooijen, S., Victor, N., and Dadi, Z.: Special Report on Emissions Scenarios: a special report of Working Group III of the Intergovernmental Panel on Climate Change, edited by: Nakicenovic, N. and Swart, R., Cambridge University Press, Cambridge, United Kingdom and New York, NY, USA, 2000.

Oleson, K. W., Dai, Y., Bonan, G., Bosilovich, M., Dickinson, R., Dirmeyer, P., Hoffman, F., Houser, P., Levis, S., Niu, G. Y., Thornton, P., Vertenstein, M., Yang, Z. L., and Zeng, X.: Technical description of the community land model (CLM), Ncar/tn-461+str, NCAR Technical Note, 2004.

Paltsev, S., Reilly, J. M., Jacoby, H. D., Eckaus, R. S., McFarland, J., Sarofim, M., Asadoorian, M., and Babiker, M.: The MIT Emissions Prediction and Policy Analysis (EPPA) Model: Version 4, MIT JPSPGC Report 125, August, 72 pp., available at: http://globalchange.mit.edu/files/document/MITJPSPGC_Rpt125.pdf, 2005.

Petoukhov, V., Claussen, M., Berger, A., Crucifix, M., Eby, M., Eliseev, A. V., Fichefet, T., Ganopolski, A., Goosse, H., Kamenkovich, I., Mokhov, I. I., Montoya, M., Mysak, L. A., Sokolov, A., Stone, P., Wang, Z., and Weaver, A. J.: EMIC Intercomparison Project (EMIP–CO_2): comparative analysis of EMIC simulations of climate, and of equilibrium and transient responses to atmospheric CO_2 doubling, Clim. Dynam., 25, 363–385, doi:10.1007/s00382-005-0042-3, 2005.

Plattner, G.-K., Knutti, R., Joos, F., Stocker, T. F., von Bloh, W., Brovkin, V., Cameron, D., Driesschaert, E., Dutkiewicz, S., Eby, M., Edwards, N. R., Fichefet, T., Hargreaves, J. C., Jones, C. D., Loutre, M. F., Matthews, H. D., Mouchet, A., Müller, S. A., Nawrath, S., Price, A., Sokolov, A., Strassmann, K. M., and Weaver, A. J.: Long-term climate commitments projected with climate-carbon cycle models, J. Climate, 21, 2721–2751, doi:10.1175/2007JCLI1905.1, 2008.

Randall, D. A., ATS14, W. R., Bony, S., Colman, R., Fichefet, T., Fyfe, J., Kattsov, V., Pitman, A., Shukla, J., Srinivasan, J., Stouffer, R. J., Sumi, A., and Taylor, K. E.: Climate Models and Their Evaluation, in: Climate Change 2007: The Physical Science Basis, Contribution of Working Group I to the Fourth Assessment Report of the Intergovernmental Panel on Climate Change, edited by: Solomon, S., Qin, D., Manning, M., Chen, Z., Marquis, M., Averyt, K. B., Tignor, M., and Miller, H. L., Cambridge University Press, Cambridge, United Kingdom and New York, NY, USA, 2007.

Raper, S., Gregory, J., and Stouffer, R.: The role of climate sensitivity and ocean heat uptake on AOGCM transient temperature response, J. Climate, 15, 124–130, doi:10.1175/1520-0442(2002)015<0124:TROCSA>2.0.CO;2, 2002.

Rayner, N. A., Parker, D. E., Horton, E. B., Folland, C. K., Alexander, L. V., Rowell, D. P., Kent, E. C., and Kaplan, A.: Global analyses of sea surface temperature, sea ice, and night marine air temperature since the late nineteenth century, J. Geophys. Res., 108, 4407, doi:10.1029/2002JD002670, 2003.

Reilly, J., Stone, P. H., Forest, C. E., Webster, M. D., Jacoby, H. D., and Prinn, R. G.: Uncertainty and climate change assessments, Science, 293, 430–433, doi:10.1126/science.1062001, 2001.

Reilly, J., Paltsev, S., Strzepek, K., Selin, N. E., Cai, Y., Nam, K.-M., Monier, E., Dutkiewicz, S., Scott, J., Webster, M., and Sokolov, A.: Valuing Climate Impacts in Integrated Assessment Models: The MIT IGSM, Climatic Change, 117, 561–573, doi:10.1007/s10584-012-0635-x, 2013.

Robine, J.-M., Cheung, S. L. K., Le Roy, S., Van Oyen, H., Griffiths, C., Michel, J.-P., and Herrmann, F. R.: Death toll exceeded 70,000 in Europe during the summer of 2003, C. R. Biol., 331, 171–178, doi:10.1016/j.crvi.2007.12.001, 2008.

Schlosser, C. A., Kicklighter, D., and Sokolov, A. P.: A global land system framework for integrated climate-change assessments, MIT JPSPGC Report 147, May, 60 pp., available at: http://globalchange.mit.edu/files/document/MITJPSPGC_Rpt147.pdf, 2007.

Schlosser, C., Gao, X., Strzepek, K., Sokolov, A. P., Forest, C. E., Awadalla, S., and Farmer, W.: Quantifying the Likelihood of Regional Climate Change: A Hybridized Approach, J. Climate, 26, 3394–3414, doi:10.1175/JCLI-D-11-00730.1, 2013.

Scott, J. R., Sokolov, A. P., Stone, P. H., and Webster, M. D.: Relative roles of climate sensitivity and forcing in defining the ocean circulation response to climate change, Clim. Dynam., 30, 441–454, 2008.

Senior, C. and Mitchell, J.: Carbon Dioxide and Climate: The Impact of Cloud Parameterization, J. Climate, 6, 393–418, doi:10.1175/1520-0442(1993)006<0393:CDACTI>2.0.CO;2, 1993.

Smith, T. M., Arkin, P. A., Ren, L., and Shen, S. S.: Improved reconstruction of global precipitation since 1900, J. Atmos. Ocean. Tech., 29, 1505–1517, 2012.

Smith, T. M., Shen, S. S. P., Ren, L., and Arkin, P. A.: Estimating Monthly Precipitation Reconstruction Uncertainty Beginning in 1900, J. Atmos. Ocean. Tech., 30, 1107–1122, doi:10.1175/JTECH-D-12-00197.1, 2013.

Sokolov, A. P.: Does Model Sensitivity to Changes in CO_2 Provide a Measure of Sensitivity to Other Forcings?, J. Climate, 19, 3294–3306, doi:10.1175/JCLI3791.1, 2006.

Sokolov, A. P. and Monier, E.: Changing the Climate Sensitivity of an Atmospheric General Circulation Model through Cloud Radiative Adjustment, J. Climate, 25, 6567–6584, doi:10.1175/JCLI-D-11-00590.1, 2012.

Sokolov, A. P. and Stone, P. H.: A flexible climate model for use in integrated assessments, Clim. Dynam., 14, 291–303, doi:10.1007/s003820050224, 1998.

Sokolov, A. P., Forest, C. E., and Stone, P. H.: Comparing oceanic heat uptake in AOGCM transient climate change experiments, J. Climate, 16, 1573–1582, doi:10.1175/1520-0442-16.10.1573, 2003.

Sokolov, A. P., Schlosser, C. A., Dutkiewicz, S., Paltsev, S., Kicklighter, D., Jacoby, H. D., Prinn, R. G., Forest, C. E., Reilly, J. M., Wang, C., Felzer, B., Sarofim, M. C., Scott, J., Stone, P. H., Melillo, J. M., and Cohen, J.: The MIT Integrated Global System Model (IGSM) Version 2: Model Description and Baseline Evaluation, MIT JPSPGC Report 124, July, 40 pp., available at: http://globalchange.mit.edu/files/document/MITJPSPGC_Rpt124.pdf, 2005.

Sokolov, A. P., Stone, P. H., Forest, C. E., Prinn, R., Sarofim, M. C., Webster, M., Paltsev, S., Schlosser, C. A., Kicklighter, D., Dutkiewicz, S., Reilly, J., Wang, C., Felzer, B., Melillo, J. M., and Jacoby, H. D.: Probabilistic Forecast for Twenty-First-Century Climate Based on Uncertainties in Emissions (Without Policy) and Climate Parameters, J. Climate, 22, 5175–5204, doi:10.1175/2009JCLI2863.1, 2009.

Stainforth, D. A., Aina, T., Christensen, C., Collins, M., Faull, N., Frame, D. J., Kettleborough, J. A., Knight, S., Martin, A., Murphy, J. M., Piani, C., Sexton, D., Smith, L. A., Spicer, R. A., Thorpe, A. J., and Allen, M. R.: Uncertainty in predictions of the climate response to rising levels of greenhouse gases, Nature, 433, 403–406, doi:10.1038/nature03301, 2005.

Stouffer, R. J., Yin, J., Gregory, J. M., Dixon, K. W., Spelman, M. J., Hurlin, W., Weaver, A. J., Eby, M., Flato, G. M., Hasumi, H., Hu, A., Jungclaus, J. H., Kamenkovich, I. V., Levermann, A., Montoya, M., Murakami, S., Nawrath, S., Oka, A., Peltier, W. R., Robitaille, D. Y., Sokolov, A., Vettoretti, G., and Weber, S.

L.: Investigating the causes of the response of the thermohaline circulation to past and future climate changes, J. Climate, 19, 1365–1387, doi:10.1175/JCLI3689.1, 2006.

Taylor, K., Stouffer, R., and Meehl, G.: An overview of CMIP5 and the experiment design, B. Am. Meteorol. Soc., 93, 485–498, 2012.

Thompson, D. and Solomon, S.: Interpretation of recent Southern Hemisphere climate change, Science, 296, 895–899, 2002.

Wang, C., Prinn, R. G., and Sokolov, A.: A global interactive chemistry and climate model: Formulation and testing, J. Geophys. Res., 103, 3399–3417, doi:10.1029/97JD03465, 1998.

Webster, M. D. and Sokolov, A. P.: A methodology for quantifying uncertainty in climate projections, Climatic Change, 46, 417–446, doi:10.1023/A:1005685317358, 2000.

Webster, M., Paltsev, S., Parsons, J., Reilly, J., and Jacoby, H.: Uncertainty in Greenhouse Emissions and Costs of Atmospheric Stabilization, MIT JPSPGC Report 165, November, 81 pp., available at: http://globalchange.mit.edu/files/document/MITJPSPGC_Rpt165.pdf, 2008.

Webster, M., Sokolov, A. P., Reilly, J. M., Forest, C. E., Paltsev, S., Schlosser, C. A., Wang, C., Kicklighter, D., Sarofim, M., Melillo, J., Prinn, R. G., and Jacoby, H. D.: Analysis of Climate Policy Targets under Uncertainty, Climatic Change, 112, 569–583, doi:10.1007/s10584-011-0260-0, 2012.

Xie, P. P. and Arkin, P. A.: Global precipitation: A 17-year monthly analysis based on gauge observations, satellite estimates, and numerical model outputs, B. Am. Meteorol. Soc., 78, 2539–2558, doi:10.1175/1520-0477(1997)078<2539:GPAYMA>2.0.CO;2, 1997.

Yokohata, T., Webb, M. J., Collins, M., Williams, K. D., Yoshimori, M., Hargreaves, J. C., and Annan, J. D.: Structural Similarities and Differences in Climate Responses to CO_2 Increase between Two Perturbed Physics Ensembles, J. Climate, 23, 1392–1410, doi:10.1175/2009JCLI2917.1, 2010.

Yu, J.-Y. and Kim, S. T.: Identification of Central-Pacific and Eastern-Pacific types of ENSO in CMIP3 models, Geophys. Res. Lett., 37, L15705, doi:10.1029/2010GL044082, 2010.

Zickfeld, K., Eby, M., Alexander, K., Weaver, A., Crespin, E., Fichefet, T., Goosse, H., Philippon-Berthier, G., Edwards, N., Holden, P., Eliseev, A., Mokhov, I., Feulner, G., Kienert, H., Perrette, M., Schneider von Deimling, T., Forest, C., Friedlingstein, P., Joos, F., Spahni, R., Steinacher, M., Kawamiya, M., Tachiiri, K., Kicklighter, D., Monier, E., Schlosser, A., Sokolov, A., Matsumoto, K., Tokos, K., Olsen, S., Pedersen, J., Ridgwell, A., Shaffer, G., Yoshimori, M., Zeng, N., and Zhao, F.: Long-term climate change commitment and reversibility: an EMIC intercomparison, J. Climate, 26, 5782–5809, doi:10.1175/JCLI-D-12-00584.1, 2013.